# Design of Polarization Reconfigurable Beam-Steerable and Frequency Tunable FPMS Based SIW-Slot Antennas

by

Saqlain Saqlain

A thesis presented to the Lakehead University in partial fulfilment of the required degree of

Master of Science

in

Electrical and Computer Engineering

Faculty of Engineering

Lakehead University

Thunder Bay, Ontario, Canada

July 2022

# ABSTRACT

With the rapid evolution of modern and smart communication technologies such as 5$^{th}$ generation of mobile network (5G), (internet of things) IoT, Autonomous Vehicles, Aviation Technology, etc., the need for reconfigurable radio frequency (RF) components cannot be emphasized enough. Thus, the rationale for plethora of research carried out in the design and development of reconfigurable/tunable RF components and devices. This work focuses on the design of a polarization reconfigurable and beam-steerable substrate integrated waveguide-slot (SIW-slot) antenna using a novel technology, field programmable microwave substrate (FPMS). At first, the antenna is optimized to operate at 4 GHz on a Duroid 5880 substrate with six slots rotated at 5° towards the center of the waveguide. This follows the integration of optimized FPMS unit cells on the slot radiators. While varying the capacitance values of the unit cells, close attention is paid to the impedance and radiation performance of the antenna. Initial results presented here show a beam steering of ~±40°. In addition, the antenna is also seen to provide gain modulation in maximum steered direction. Interestingly, as the antenna radiation is steered, the polarization of the antenna switches from $\boldsymbol{E_{\varphi}}$ (maximum at 0°) to $\boldsymbol{E_{\theta}}$ (±40°). This makes the design an excellent candidate for end-to-end secured communication with minimum interference in applications such as aircraft RADARs. Thus, the antenna performance metrics show the promise of the unique FPMS technology in designing of smart RF components.

**Keywords:** Substrate Integrated Waveguide (SIW) slot antenna; Field Programmable Microwave Substrate (FPMS); Linear Polarization (LP); Circular Polarization (CP).

# ACKNOWLEDGEMENT

*In the name of Allah, Most Gracious, Most Merciful.*

*Praise be to Allah, the Cherisher and Sustainer of the Worlds. First and foremost, I am very grateful to my God for his blessings and graces. Who gave me the strength and determination to complete this study that without him it would not have been accomplished.*

*No words of thanks can sum up the gratitude that I owe to my research supervisor Dr. Farhan Abdul Ghaffar for his unlimited support, guidance, and continuous advice during my research activities. His scholarly advice, meticulous scrutiny, and scientific approach melded with a deep understanding of the subject has been solely and mainly responsible for the completion of this research work. His emotional support, guidance and belief in me during the tough times of pandemic were invaluable and contributed to my success. He has taught me the methodology to carry out the research and to present the research work as clearly as possible. It has been a great pleasure and honor to have him as my supervisor. I also wish to acknowledge Dr. Farhan Abdul Ghaffar for the financial support to conduct this work. Also, I would like to thank the committee for their valuable suggestions and support.*

*My family and friends, in particular, my father Muhammad Razzaq, my mother Samara Razzaq and my aunt Samia Sheikh as well deserve a special mention for their continued prayers for my success and for their love, caring and sacrifices for educating and preparing me for my future. Also, I express my heartiest gratitude to my sisters, brother and my fiancée, for their support and valuable prayers.*

*My sincere appreciation also goes to Noben Roy Kumar who has helped me directly or indirectly in the completion of my thesis and research, as well as the CMC Microsystems team members for their help and support with the Ansys software for simulation*

# TABLE OF CONTENTS

# LIST OF FIGURES

## Chapter 1



## Chapter 2

## Chapter 3

## Chapter 4

## Chapter 5

# Chapter 1: Introduction

## 1.1 Motivation

To accommodate the rapid growth of wireless communications and the need to integrate different wireless standards on a single platform, radio frequency (RF) circuits must be designed to have reconfigurable performance characteristics [19]. Components such as antenna front-ends need to be frequency tunable, polarization reconfigurable, beam steerable, etc. To meet the needs of modern applications, such as satellite and space communications, autonomous vehicles (AV), military radars, IoT, and 5G systems antenna designs with agile impedance and radiation characteristics are required that can satisfy the operational needs of host system [2], [19].

Reconfigurable antennas find their application in modern wireless systems due to the rapid advancement of technology. For instance, in satellite and space communication, reconfigurability is a compulsion without which the system will not perform as intended. The movement of the satellite relative to the base station on the ground means that the antenna beam needs to steer in order to establish a wireless communication link between the two [2]. Likewise, in a surveillance radar system for military defense, the targets to be detected are usually in motion, necessitating antenna system adaptability in order to identify the targets, as depicted in Fig. 1.1. The requirements of these applications are such that they need reconfigurable antennas that can steer the beam.

Classically, radar and satellite communication systems have been used for decades [20]. However, the modern version of these applications has new challenges that previous systems did not have. Since their inception, most of these systems have been bulky, large, and primitive. The current

wireless systems have their own set of challenges such as compact size, multi-functionality, low cost, and last but not the least improved efficiency.

(a) (b) (c)

Figure 1.1: Applications of Reconfigurable Antennas (a) Satellite and Space Communication (b) Surveillance Radar (c) Military Radar Base Station [1], [2]

For example, modern concept of satellite communication requires different satellites to connect with each other to exchange information. Antenna of the satellite as shown in Fig. 1.2(b) propagates a high-power EM wave along the specified direction marked in solid lines. In order to cover all the devices satellite needs multidirectional propagation. Similarly, as depicted in Fig. 1.2(a) the target (car) is continuously in motion with respect to the antenna tower, unlike the previous example in which the base station was fixed and this is the reason to add new feature to our antenna component.

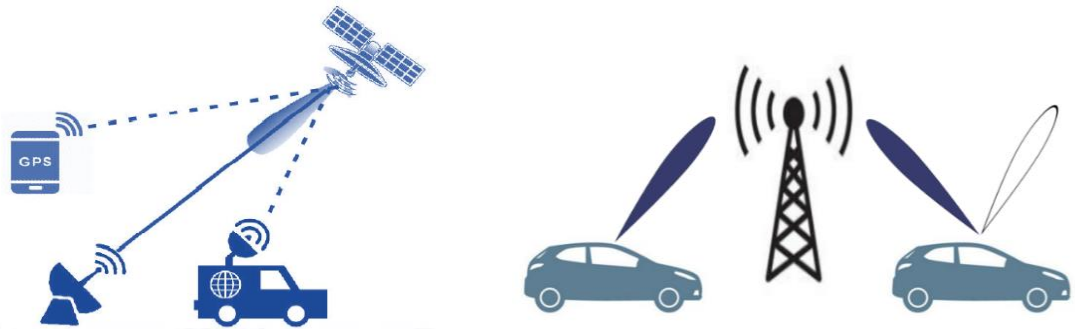


(a) (b)

Figure 1.2: Modern Applications (a) Satellite communication to cover various targets (b) On-The-Move Vehicular System [3], [4]

The transformation of these applications from their old selves to the newer versions is evident from some of the examples shown in Fig. 1.2 [3], [4]. As has been established that these systems need reconfigurable RF components such as antennas that are frequency tunable or radiation pattern reconfigurable.

The aforementioned wireless applications require smart antenna systems. As the number of wireless applications increased, the necessity to combine many functionalities into a single system has surfaced. This integration decreases the size, weight, price, and volume. This integration includes antennas, hence reconfigurable antennas have garnered substantial attention. They are low-cost promising solutions that can change their properties to adapt to their surroundings and meet operational requirements. The most common types of reconfigurable antennas are frequency tunable, radiation pattern, and polarization reconfigurable.

Frequency-tunable antennas are designed to have a center frequency that may be altered according to the needs [21]. These are useful when multiple communication systems overlap in a single [22], [23] solution like the smart gadgets of today. These communication devices operate at different standards such as Wi-Fi, global system for mobile communication (GSM), global positioning system (GPS), Bluetooth, etc. [22], [23]. If a single antenna can be designed to cover all these frequency bands, then it can avoid the use of multiple antennas in a single system. A solution of this sort contributes the size and cost reduction while maintaining the performance standards [24].

Correspondingly, radiation pattern reconfigurability can be achieved by modifying the spherical distribution of the antenna's radiation. This includes beam steering, polarization, and pattern reconfigurability. Beam steering, which involves directing the path of the maximum radiation (main lobe) to optimize antenna gain in a particular direction, is the most commonly used application in this instance. There have been numerous implementations of beam-scanning antenna arrays in

various technologies over the years (waveguides, microstrip, and so on)[25]–[27]. Among these, the SIW concept has become a popular platform for realizing antennas and circuits over the past decade [28]. SIWs combines the simplicity and low loss nature of rectangular waveguides with the low cost, ease of fabrication, and compatibility with planar circuitry. With the help of this technology, the designers have reported beam scanning antennas by integrating phase shifters between antenna elements [29] which are known as the conventional method. The other technique is by using traveling wave antennas that can steer the antenna beam by changing the frequency of the input signal [15].

Similarly, polarization reconfigurable antennas switch between different polarizations, i.e., from linear polarization to circular polarization and vice versa, or from vertical polarization to horizontal polarization, etc. This feature can be used for a variety of reasons, including improving system capacity, minimizing multipath effects in wireless channels, and polarization coding for digital systems [30]–[32]. In general, there are two main approaches to achieving reconfigurable polarizations for Circular polarize (CP) antennas: reconfigurable radiating element and reconfigurable feeding network [33].

Thus, beam steering and polarization reconfigurability in antennas are important aspects that can meet the versatility of the modern wireless application. The focus of this thesis is on the design of a fixed frequency polarization reconfigurable, beam steerable SIW slot antenna using a novel technology known as FPMS [18]. FPMS is being studied for the first time in a SIW-slot antenna as it has been used to demonstrate beam steering in a microstrip-based leaky-wave antenna (MLWA), previously [34]. FPMS is made up of discrete unit cells that can control the dielectric characteristics of a medium locally. This makes it an ideal platform for the design of slotted SIW antennas, which depend on the substrate's progressive qualities to create the required radiation characteristics. The slotted SIW with integrated FPMS unit cell is the focus of this work.

## 1.2 Thesis Objective

The thesis objectives can be summarized as follows

- To employ of FPMS technology in a SIW-slot antenna for the first time.
- Moving slightly higher in frequency as compared to the existing literature in FPMS technology.
- To study the beam steering capabilities of the FPMS-based slotted SIW antenna.
- Investigate polarization reconfigurability in the antenna under study.
- The integration of FPMS could provide frequency control to the designer. This is another aspect to be evaluated through this work.

## 1.3 Thesis Contribution

From the proposed thesis research, the following contributions can be outlined:

- First-ever slotted-SIW antenna based on FPMS technology is presented in this work.
- A beam scanning range of ±42º is achieved from the full-wave simulations carried out in an electromagnetic (EM) simulator (Ansys High-Frequency Structure Simulator, HFSS).
- A progressively shifting polarization with maximum $E_\theta$ at ±42º and maximum $E_\varphi$ at -4º has been accomplished.
- The antenna has a maximum gain of 6 dBi and a gain fluctuation of 2 dB when the primary beam is steered to a maximum of ±42º, i.e., on either side of the azimuth plane.
- Integration of FPMS unit cells near the feed of the antenna provides frequency tuning with stable gain and radiation performance at 4 GHz.

## 1.4 Thesis Organization

In the first chapter, a literature survey of reconfigurable antennas and their most prevalent forms is presented. Figure 1.2 explains the requirement for reconfigurable antennas in contemporary applications. The motivation for this thesis is then clearly articulated.

In the second chapter, a brief introduction to the SIW technology is presented that extends into the integration of slot radiators into the waveguide structure. Relevant research articles that use this type of antenna are covered along with the merits of the design and the novelty introduced by the researchers.

Chapter 3 begins with an introduction to the FPMS technology and its unit cells that are needed to realize it. This is followed by a detailed discussion on the optimization of the FPMS unit cells with respect to the dielectric constant and the resonant frequency, which is done by varying different design parameters and studying the impedance results.

In chapter 4, a novel reconfigurable technology known as FPMS for the construction of a beam steerable SIW slot antenna has been investigated. At first, the chosen antenna design is optimized to work at 4 GHz in term of radiation pattern with the help of a full wave solver ANSYS HFSS. The integration of the optimized FPMS unit cells in the slots of the antenna is then carried out. Followed by a complete parametric study is performed on various design parameters to obtain the best possible impedance and radiation performance of the antenna.

Finally, the thesis concludes by listing the contributions of this work and highlighting some of the future steps that are currently undertaken to validate the proposed design in measurements. Furthermore, other research directions on the antenna design using FPMS technology are also explained briefly to hint at possible future initiatives.

# Chapter 2

## Background and Literature Review

The thesis focuses on the design of beam-steerable/reconfigurable antennas with a special focus on SIW-based slot antennas, therefore, it is pertinent to dwell on the operating principle of this class of antenna. Furthermore, a brief summary of the designs that already exist in the literature is covered in this chapter.

### 2.1 SIW Structure

Waveguides have been classically used in the design of RF and microwave components due to their low loss performance. In the recent past, a potent substitute to the metallic waveguides was introduced in the form of a SIW structure. It consists of two-conductor planes at the top and bottom layers of the substrate with the vertical walls designed with the help of rows of conductor vias embedded in a dielectric substrate [9]. This results in the replacement of the vertical metallic walls with a series of vias and allows the non-planar rectangular waveguide to be transformed into a planar shape that is compatible with conventional planar processing techniques. SIW structures retain the majority of the properties of typical rectangular metallic waveguides. For instance, their propagation characteristics, such as the field pattern and dispersion characteristics, are comparable to those of conventional rectangular waveguides. With the employment of a low-loss dielectric substrate, the designer can maintain good RF transmission through the guide with reasonably high-power handling capabilities. The idea of a SIW structure has been initially introduced in the early 1990s, however, the concept gains a lot of attention in the mid-2000s [9], [35]–[37].

Cassiviet in 2002 analyzed the dispersion properties of SIWs using the Boundary Integral-Resonant Mode Expansion (BI-RME) method in conjunction with Floquet's theorem [5]. It is well known that SIW is a periodic structure that is realized by repeating its fundamental unit structure, shown in Fig. 2.1, where Fig. 2.1(a) shows the complete structure with Fig. 2.1(b) showing the fundamental unit structure. Using the BI-RME approach, a generalized admittance matrix of the periodic cell is determined. With the help of Floquet's theorem, one can easily determine the eigenvalues of the structure. The eigenvalues represent the propagation constants of the TE (transverse electric) modes propagating through the SIW, whilst the eigenvectors represent the pattern of the modal fields. In the domain of RF design, these are commonly known aspects of SIW design and have been used for the last two decades. With the help of this complete analysis, the authors in [5] have theoretically established that the SIW structure is no different from rectangular waveguides in terms of wave propagation.

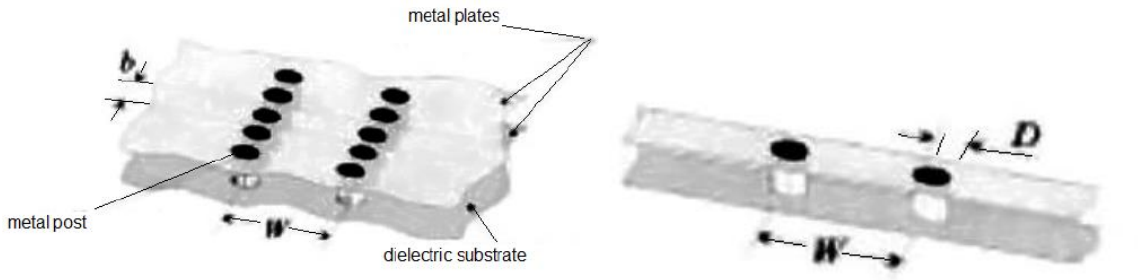


Figure 2.1: (a) Sketch of SIW (b) Periodic cell of SIW [5]

Theoretically, SIWs do not differ from rectangular waveguides, however, their implementation has its own set of challenges and at times can be more difficult than traditional waveguides. Deslandes and Wu have established a basic design technique that converts a SIW into a rectangular waveguide [38]. The authors have developed a method for finding the complex propagation constant of a SIW using the idea of surface impedance to represent the rows of conducting cylinders that serve as the

sidewalls of a SIW. Using the Method of Moments (MoM) and transverse resonance, the proposed model is solved. An electromagnetic wave of a TE mode wave propagating via a waveguide can be described by the superposition of two waves propagating in the direction of energy propagation [38]. Surface impedance $Z_s$ can be used to indicate each via hole row. An important aspect of SIW is that it does not have physically continuous walls that act as PECs, because no matter how small the distance there will be some gap between the consecutive vias. One should keep in mind that electrically this gap could be small for the wave to emanate through it. In any case, due to the physical difference between the rectangular waveguides and SIW, there is a slight difference in the calculation of the guide's dimensions. With the help of MoM, the gap between the vias can be optimized to minimize the leakage of the wave. This will in turn also affect the input reflection coefficient. With the advent of modern EM simulators, this step has been greatly simplified. However, there are certain basic criteria that are to be met in order for the structure to be viable. These are: 1) the separation distance ($b$) must be greater than the diameter of the via hole ($D$) but it should be less than $2D$ and 2) the distance between the vias ($b$) should be less than the quarter of a wavelength at cut off frequency. These theoretical limitations have been validated by the authors in [38] by the actual implementation of SIW structure and comparing the results of the two. Therefore, it provides good guidelines for the designers planning to use SIW as an alternate to rectangular waveguide structures.

## 2.2 Classical Waveguide-based Slot Antennas

Although the focus of this work is on SIW-based designs, it is pertinent to start the discussion of slot antennas realized using conventional waveguides. Fundamentally speaking a slot antenna belongs to the class of aperture antenna. An aperture antenna is realized by cutting to create a rectangular or

square slot into an infinite sheet of the conductor. Making a cut of known dimensions on the surface of the antenna's mounting plate is all it takes to create these slot antennas. Slot antennas usually radiate in an omnidirectional fashion with some similarity to electric dipole and loop antennas. Using this basic concept of an aperture or slot radiator, waveguide-based slot antennas have been introduced by RF designers. In the case of waveguide or SIW slot radiators, it is recommended to use an array of slots instead of a single radiator. The inception of this concept happened in 1943 at McGill University in Montreal. Unique features of these antennas are horizontal polarization and omnidirectional gain around the azimuth. To control the electrical behaviour in terms of radiation and internal impedance length, position, inclination, and width of the slot can be modified [39].

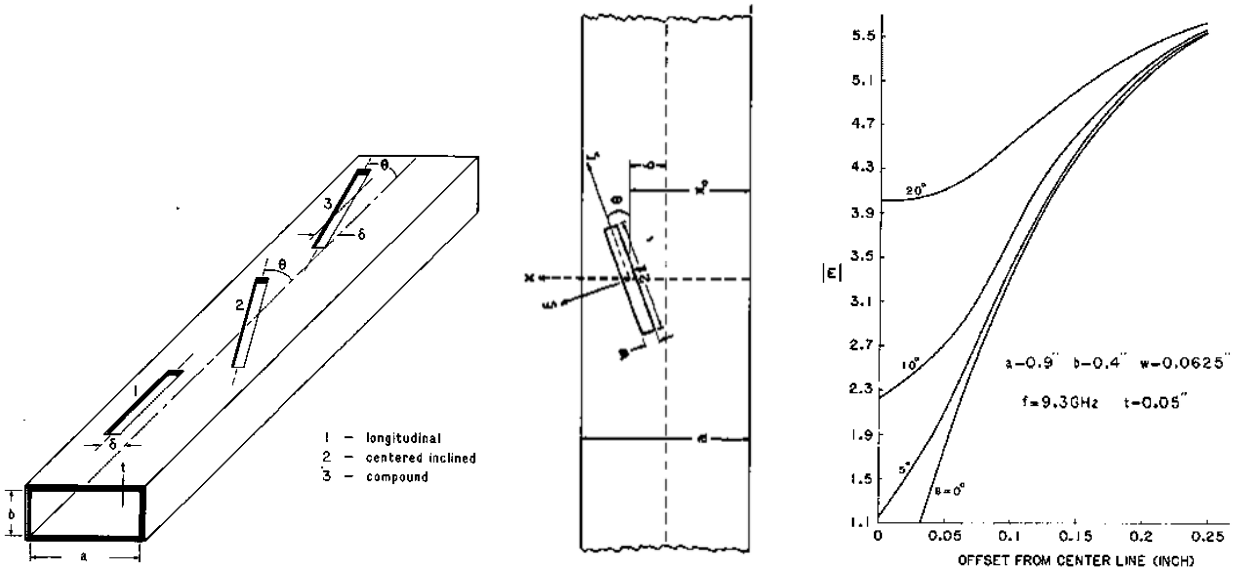


(a) (b) (c)

Figure 2.2: Broad wall rectangular waveguide (a) Broad wall radiating slots (b) Geometry of compound slot (c) Magnitude of aperture electric field at resonance [6]

The optimized orientation of the slot is such that its length should be parallel to the propagation of the wave. However, the effect of offset and tilting of radiating slot in a waveguide has been studied analyzed by Rangarajan in 1989 [6]. Rangarajan [6] contributed to the employment of centered-

inclined and compound slots to characterize them in terms of radiation purpose. A few orientations of the slots on a rectangular waveguide has been shown in Fig. 2.2(a). Method of Moments (MoM) in conjunction with the Green function is employed to calculate the fields on the apertures of the slot. The advantage of the compound slot array compared to the center-inclined slot array is that the spacing between elements is reduced to approximately half guided wavelength as compared to full guided wavelength. In addition, small offsets cause the compound slot to operate primarily as a centered inclined series element with a considerable tilt dependence, whereas large offsets imply its behavior as a shunt element with a relatively low tilt sensitivity. This study concluded that the structural factors of the slot play an important role in the overall gain, side lobe, and impedance performance of the antenna [40].

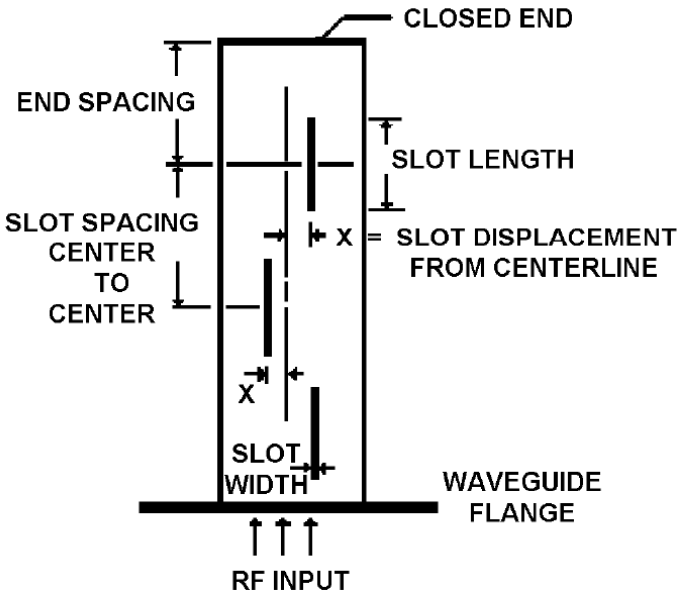


Figure 2.3: Waveguide Slot Antenna [7]

A detailed discussion on the theory and implementation of slot array antennas realized on a rectangular metallic waveguide is presented in [7]. Rather than focussing on individual publications, one can read through this reference to understand not only the functionality of such an antenna design

but its limitations and implementation constraints. Like in Fig. 2.4 the author explains how the placement of slot at different locations in the waveguide will result in the RF radiation performance. For instance, slot ***g*** is designed in a manner that, it is aligned with the direction of the sidewall current, thus it does not radiate. Similarly, no radiation is observed from slot ***h*** since the transverse current is zero. Slots ***b***, ***c***, ***i*** and ***j*** are shunt slots due to the fact that they interrupt the transverse currents ($J_x$, $J_y$) and can be represented as two-terminal shunt admittances. Slots ***e***, ***k***, and ***d*** are represented by series impedance and interrupt $J_z$. Slot ***d*** interrupts $J_x$, but the excitation polarity on either side of the waveguide's center line is opposite, prohibiting radiation from that current component. Both $J_x$ and $J_z$ excite slot ***f*** to radiate [8]. To sum up, the authors of the book nicely summarize that how a designer can introduce slots in the various locations of a rectangular waveguide and what to anticipate from the resultant change in structure. It is worth mentioning here that any of the slots along the vertical walls of the waveguide are of no use for a SIW structure. Therefore, in this work, the focus is on the slots in the upper conductor of the waveguide or SIW structure that will be covered in the next section.

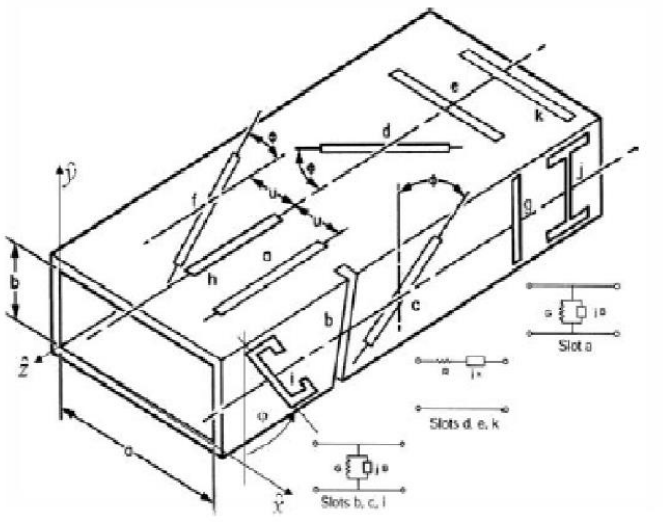


Figure 2.4: Slots cut in the walls of a rectangular waveguide [8].

## 2.3 SIW with slots:

The first study on waveguides slots can be traced back to the 1940s [41], but their inherent advantages (e.g., feed and radiating elements integrated into the same structure, low insertion loss, tunable radiation pattern, low cross-polarization levels, and ease of fabrication) granted them long-lasting popularity that has remained to this day [42].

The slot is actually a cut along the length of the waveguide, this interrupts the transverse current flow in the conductor layer and compels it to travel around the slot. As a result, the electric field patterns as shown in Fig. 2.5 (b). The location of the slot in the rectangular waveguide determines the flow of current and the resultant radiation characteristics. Consequently, the position of the slot dictates the impedance experienced by the propagating RF wave as well as the quantity of energy coupled and radiated by the slot [43], [44]. By changing the physical properties of the slot (i.e., length, width, and its position) and the dimensions of the SIW structure, one can optimize the radiation and impedance performance of the SIW slot antenna [38], [45].

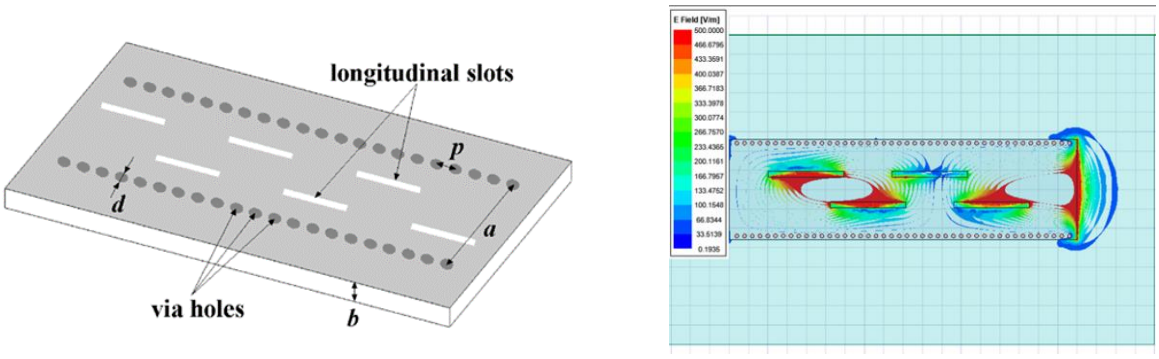


(a) (b)

Figure 2.5: SIW Slot Antenna (a) Configuration of a substrate integrated waveguide [9] (b) Electric field distribution in slotted SIW

## 2.4 SIW with different Slot configuration

The placement of slots in a waveguide structure arranged in a longitudinal fashion generates the best radiation characteristics. The geometry thus achieved provides merits such as low cross-polarization levels and improved efficiencies [6]–[8]. This pattern of slot placement has been extended to SIW structures as well. Elliot et.al, in his publication [39], provided an extensive study on how the slot alignment along the broad wall of rectangular waveguides affects the resultant radiation. This work formed the basis for this class of antennas. Extrapolating on this work, Hosseininejad et al. in [10] proposed a SIW-slot antenna with 10 slot elements, shown in Fig. 2.6(a). The entire antenna and feeding system are combined on a single substrate, resulting in a compact, low-profile, and low-cost design. The top metallic surface of a SIW was etched with longitudinal slots, which are slightly displaced from the center of the waveguide. In addition, they developed an optimal design approach for the SIW-slot antenna by employing the Method of Least Squares (MLS). A four-term error function is formulated, including terms for the design equations, input impedance matching, pattern synthesis, and the load power dissipation. The error function is then minimized in relation to the design parameters (slot lengths, offsets, spacings, and excitations) by using a combination of the genetic algorithm and conjugate gradient method (GA-CG). The optimized antenna design shows a simulated gain of 13.4 dBi, while the measurement of the fabricated prototype results in a maximum gain of 12.35 dBi. These results are observed at the center frequency of 10 GHz with an impedance bandwidth of  8%. Thus, the design shows good impedance and radiation characteristics that are generally expected from a SIW slot antenna.

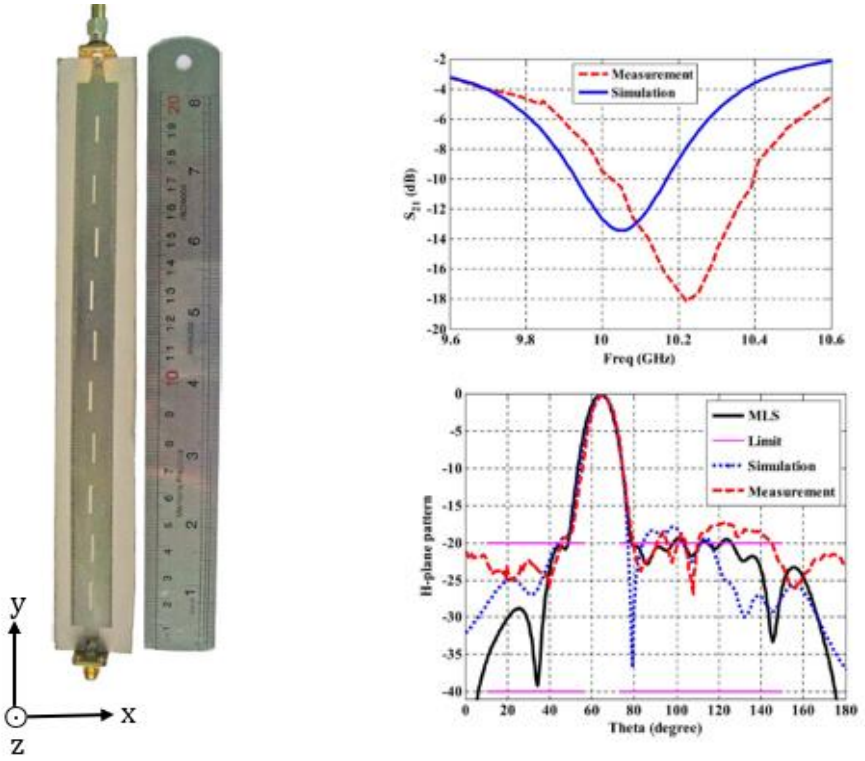


(a) (b)

Figure 2.6: (a) Fabricated design of antenna (b) S-parameters and *H*-Plane radiation plots at 10GHz [10]

Similar to [10], another antenna design that proposes to reduce the side lobe level (SLL) of antenna radiation is presented in 2019 [11]. The suggested antenna achieves a lower SLL when compared to the traditional SIW slot array. The antenna consists of three primary components: a dielectric substrate, a coaxial port, and a matched load. The antenna has 13 radiating slots as can be seen in Fig. 2.7 (a), and the space between adjacent slots is higher than half the wavelength of the antenna operating frequency, thus the main beam is skewed toward the load. As evaluated, the antenna achieved a maximum radiation at 26º from the boresight and a SLL of greater than 20 dB as compared to the maximum gain between 35.2 and 35.8 GHz. These results validate the design proposed by the authors achieves the desired goals. A similar research on this class of antenna is published by another

group of researchers that tried to optimize the SLL of the antenna structure [12]. In this method, amplitude distribution is enforced in the slots by progressively narrowing the SIW width. As shown in Fig. 2.8(b), the SIW with tapered width can be realized efficiently by altering the position of the side-wall vias. The novel approach has been validated on a 12-element SIW slot array in millimeter-wave band of frequency spectrum i.e. 94 GHz with SLL values as low as 30 dB below the antenna gain.

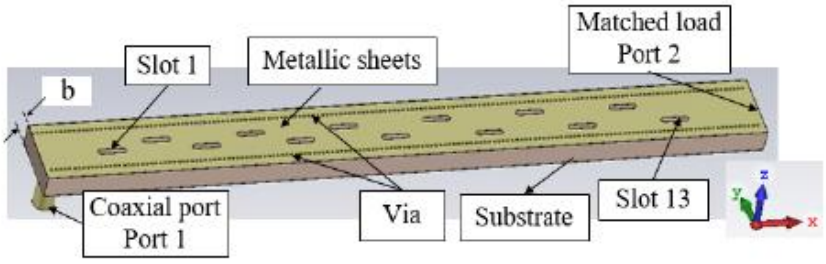


(a)

(b)

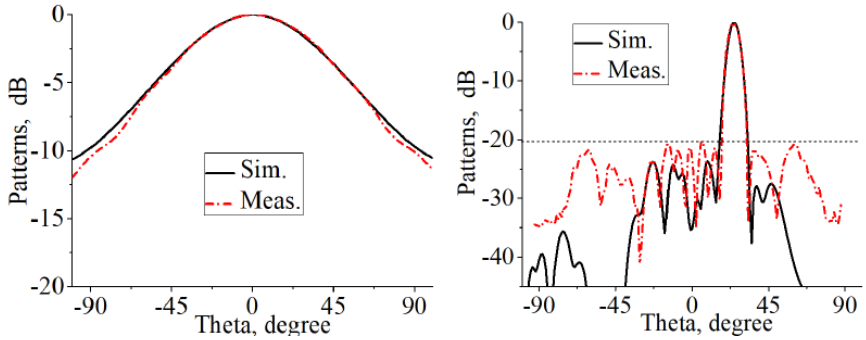


(c) (d)

Figure 2.7: (a) Configuration of the proposed antenna.(3-D view) (b) Fabricated design (c) E-plane radiation plot at 35.2GHz (d) H-Plane radiation plot at 35.2GHz [11]

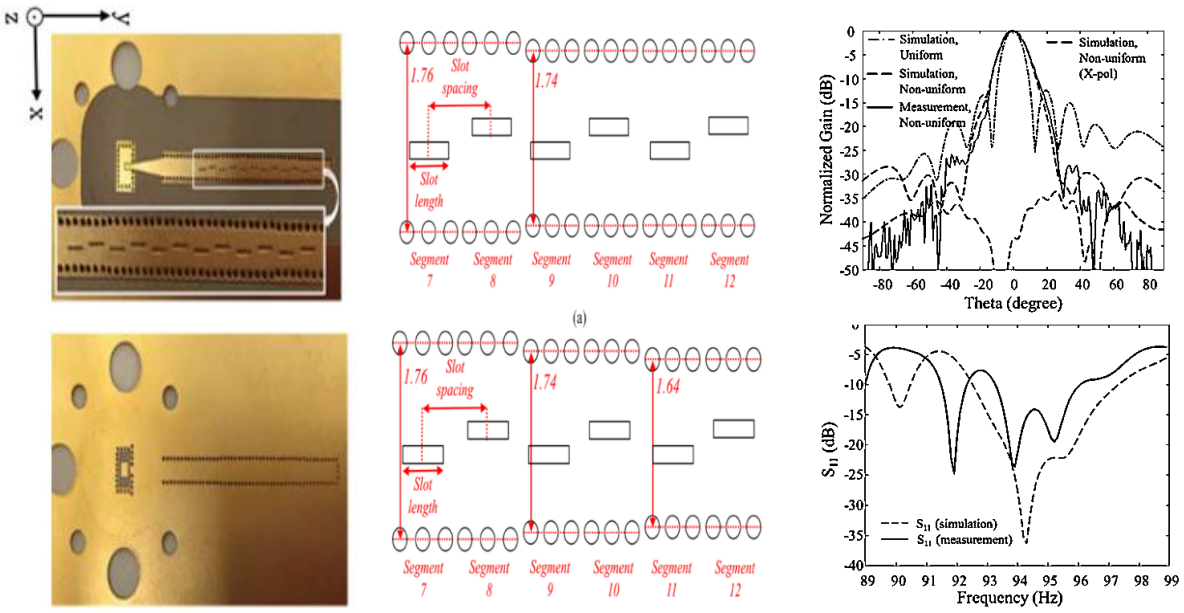


(a) (b) (c)

Figure 2.8: (a) Fabricated SIW antenna (b) SIW Antenna with tapered widths by changing distance between vias (c) Measure and Simulated Radiation and S-parameters plot [12].

Most of the designs that have been reported here are focused on linearly polarized (LP) antenna radiation. Generally, this is the type of radiation one expects to observe from SIW-based slot radiators. However, in [13] the authors introduced a circularly polarized (CP) SIW slot radiator as shown in Fig. 2.9(a). Due to the arrangement of the compound slot pair, the slot radiator's reflection is extremely weak, which simplifies the linear traveling wave design. On the basis of this construction, a 16-element CP SIW traveling wave antenna is built, manufactured, and finally characterized at 16 GHz. Experimentally, a side lobe level (SLL) of -23 dB is achieved when compared to the normalized gain of the antenna, with an axial ratio (AR) (ratio between the major and minor axis of a circularly polarized antenna pattern) of 1.95, Fig. 2.9(b). This design is quite intriguing because of its unique radiation properties that is generally not seen in SIW slot antenna elements.

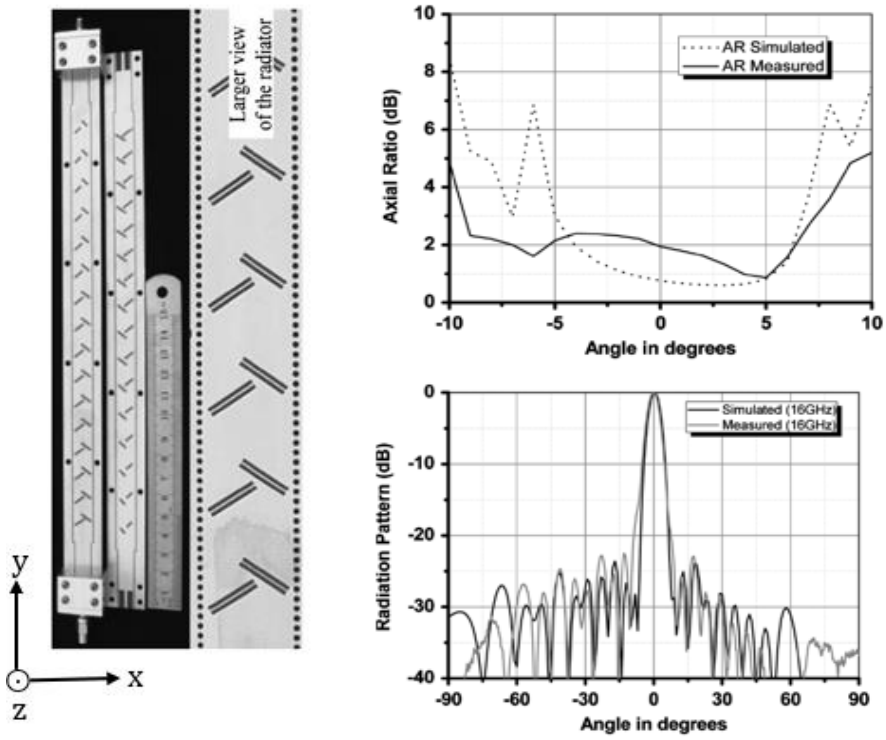


(a) (b)

Figure 2.9: (a) Different cross-section views for 16 slot elements (b) Axial Ratio plot at 16GHz followed by measured and simulated radiation plots [13]

Focussing on the polarization characteristics of the antenna, another design that is worthy of discussion is reported by Kim, *et. al.,*[14]. By using an arrangement of alternating inductive and capacitive loaded slot pairs, sixteen radiating slots are spaced by one-half of a guided wavelength in each direction. The geometry of the proposed antenna is shown in Fig. 2.10(a). This innovative antenna is able to achieve impedance matching, uniform field excitation, and suppression of grating lobes concurrently due to the alternating reactance slot pairs. The measured impedance bandwidth, maximum gain, and sidelobe levels at the design frequency 34.6 GHz are 2.7%, 15.64 dBi, and 15.36 dB, respectively.

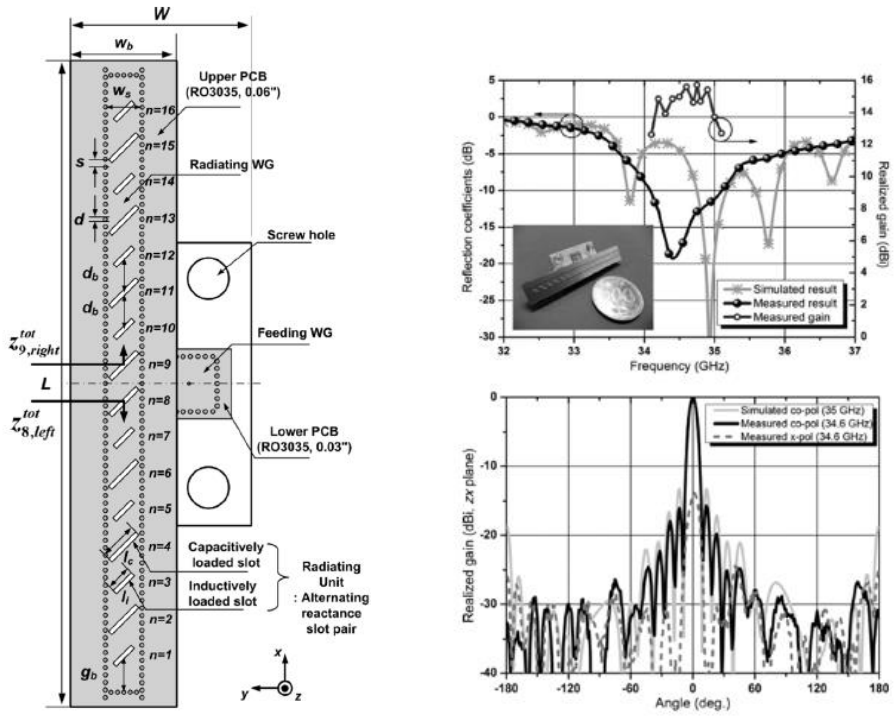


(a) (b)

Figure 2.10: (a) Geometry of the proposed SIW series slot antenna. (b) Reflection coefficients and realized gain results followed by Simulated and measured radiation patterns in *zx*-plane [14]

This section has summarized a few of the most recent antenna design that shows how SIW-based slot antenna elements are used by RF designers to achieve desired radiation characteristics. Most of the designs show efficient gain and bandwidth performance that is usually anticipated from antenna elements. It is interesting to note here that this class of antennae actually relies on an array of slots linearly spaced from each other. However, none of the researchers focused on studying beam steering from these antenna designs, which is generally investigated in structures that rely on arrays. In fact, in order to achieve beam steering, it is mostly seen that phase shifters are integrated into the antenna system. This characteristic of SIW-based slot antenna arrays is to be covered in the next section which will eventually formulate the research problem for this thesis.

## 2.5 Beam-steering in SIW Slot Antenna

As discussed in the last section, single SIW slot antenna structures do not provide the advantage of beam scanning or steering. Here it would be important to focus on some designs that rely on array theory to demonstrate beam steering. The first being [15] where the authors use the principles of antenna arrays to realize a reconfigurable radiating antenna. With the help of 'Phase Grating Method, the authors looked into steering the main beam by varying the input frequency of the RF signal. The beam scanning angle range is broadened by meandering the entire feeding structure, and the gain is increased by a metallic grating cover functioning as a 1-D lens, shown in Fig. 2.11.

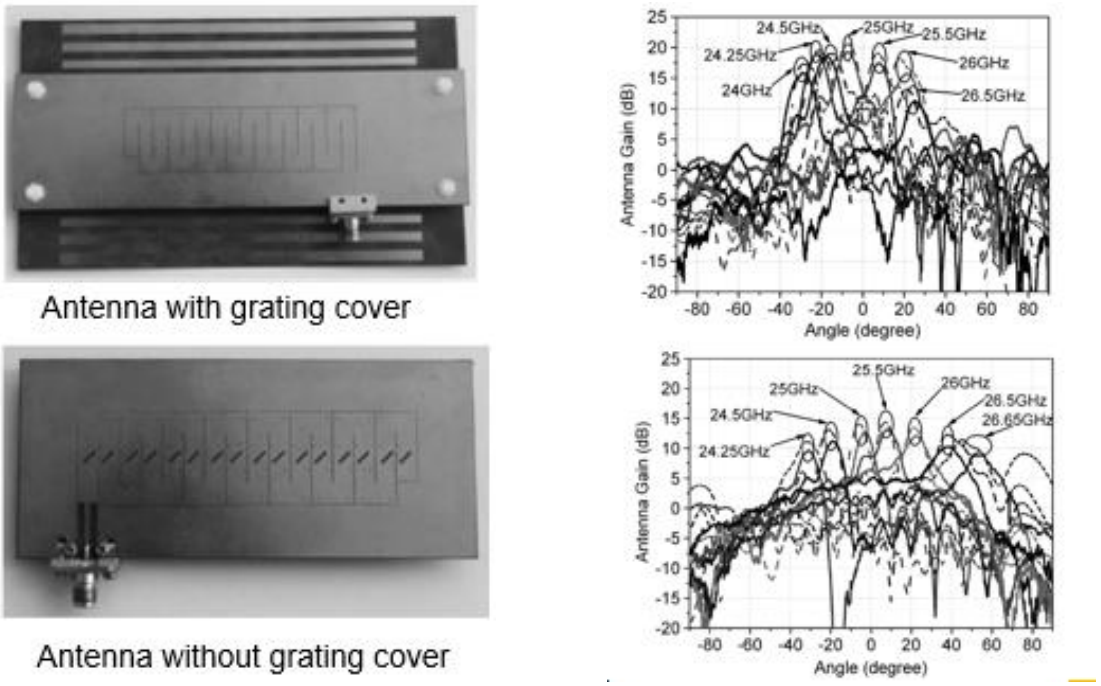


(a) (b)

Figure 2.11: (a) Fabricated Antennas (b) Simulated (dashed) and measured (solid) radiation patterns [15]

The antenna radiates well over the band of 24 to 26.5 GHz with a gain variation of 5-7 dB which is acceptable since the maximum gain of the antenna is around 20 dB. However, the main downside of this antenna is that its beam steering capabilities are not achieved at a single frequency of operation. Rather, one needs to change the excitation signal frequency to see the gain steer over the boresight of the antenna structure. This is not a desirable trait. It would be pertinent to study these antennas where the radiation can be steered at a single frequency.

A better design that can provide fixed frequency beam steering using SIW slot elements is reported in [16]. Traditional 1×8 planar phased array with integrated active phase shifters is used to achieve the desired reconfigurability. The proposed antenna is built on a single-layer substrate whose back is completely covered by a metal ground. The top metal layer is etched with four inclined slots in accordance with the requirements of a rectangular waveguide slot antenna as illustrated in Fig.2.12(a).

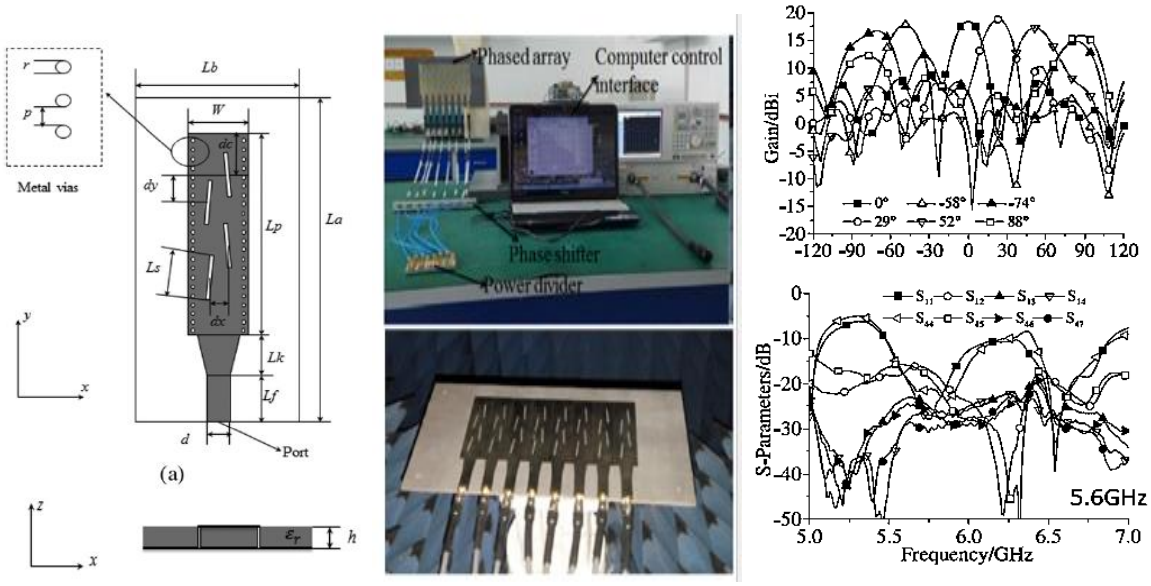


(a) (b) (c)

Figure 2.12: (a) Antenna under Study (b) Fabricated 1×8 phased (c) Radiation pattern and S-Parameter at 5.6GHz [16]

The electric fields in the slots function as equivalent magnetic currents. In contrast to conventional microstrip antennas, the equivalent magnetic currents from slots across a bigger metal ground can radiate with a broad beamwidth. With a relative impedance bandwidth of 17.7 %, its operating range is shown to be 5.40 GHz - 6.45 GHz. Beam scanning range of -74° ~ +88° was also achieved with a maximum gain of 17.3 dBi. The array is shown to steer the beam with the range of -74° to +88°, which is quite impressive. It means that the antenna system can approximately cater for the entire elevation range above the antenna plane. These results are summarized alongside the measurement set up in Fig. 2.12 (b) and (c).

Another excellent illustration of beam steering in a SIW slot array antenna is shown in [17]. In contrast to current popular methods for creating SIW phased arrays, which rely on surface-mount components (p-i-n diodes, phase shifters, etc.) for controlling the phase of the individual antenna elements, the phase is controlled in this design by using magnetic reconfigurability. The phase shifter is designed on a multilayer ferrite substrate that can be controlled by the application of an external magnetic field, Fig. 2.13 (a). With the help of external bias windings, the prototype demonstrates a maximum E-plane beam-scanning of ±28° with a stable gain of 4.9 dBi at 13.2 GHz., Fig. 2.13 (b) and (c) In addition, the array can Also operate with embedded bias windings as opposed to external ones. This is of great benefit to achieving the desired miniaturization. However, this quality is only seen at the expense of the beam steering range. Nevertheless, stable gain and radiation performance is seen from a SIW slot antenna that is designed on a magnetic material.

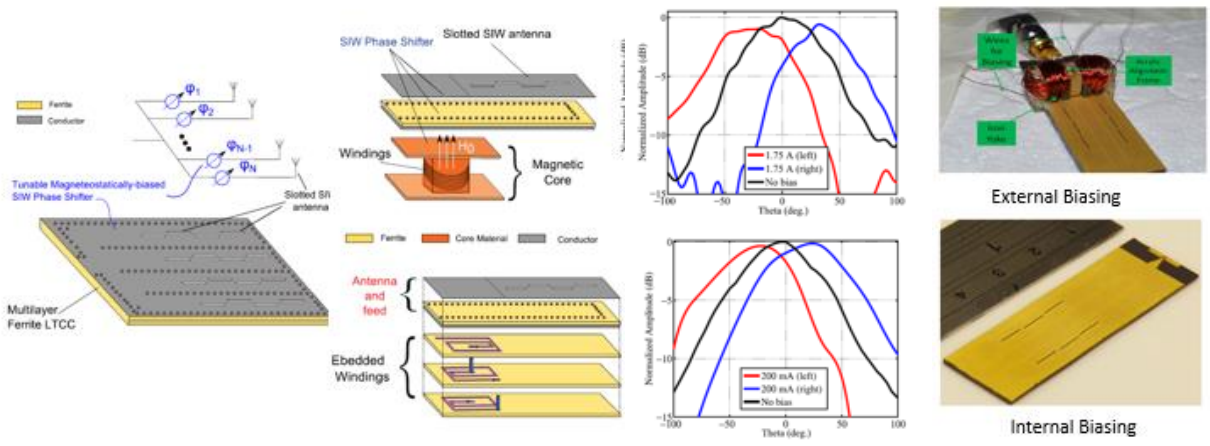


(a) (b) (c)

Figure 2.13: (a) Design of Ferrite LTCC Based SIW Phased Antenna Array (b) Resultant Radiation Pattern for external and internal biasing (c) Fabricated Antennas [17]

The group of antennas from the literature that is summarized in this section relies on external phase shifters to achieve beam steering from SIW slot antennas. To the author's knowledge, none of the antenna designs that use SIW slot radiators show beam steering capability in the absence of external phase shifters. The absence of such an antenna design is the basis of research for this thesis. It is quite appropriate to investigate a design that can steer the antenna beam without relying on external phase shifters. Using a novel FPMS technology, this idea is to be explored here and will be discussed in detail in the consequent chapters.

## 2.6 Conclusion

This chapter begins with the fundamental discussion on the operating principle of SIW antenna design in order to understand the antenna's radiation properties. A brief introduction to the SIW technology is presented that extends into the integration of slot radiators into the waveguide structure. Few research articles that use this type of antenna are covered along with the merits of the design and

the novelty introduced by the researchers. The chapter concludes by showing that reconfigurability of SIW slot antennas is achieved by designing arrays that rely on integrated phase shifters This is a very classical approach and results in designs that are bulky and hard to handle. Therefore, there is a clear need to investigate beam steering from SIW slot antennas using other methods. Since the antenna itself consists of an array of slot radiators, it is compelling to see if the phase performance of these slots can be controlled to achieve beam steering from a single SIW slot antenna rather than an array. Consequently, the author intends to investigate a novel reconfigurable technology known as FPMS for the construction of a beam-steerable SIW slot antenna in this thesis.

# Chapter 3

## Field Programmable Microwave Substrate

The second chapter of this thesis goes into the details of the slotted SIW design, beginning with the discussion on operating principles of SIW structure, which extended into the design of SIW-based slot antennas, and then concluding with an important aspect of beam steerability in these designs. From this study, it is derived that reconfigurability in slot-based SIW antennas is achieved by designing arrays rather than using a single antenna element. Consequently, the primary objective of this thesis is to demonstrate reconfigurability from slotted SIW structures in terms of their impedance and radiation characteristics. Reconfigurability can be achieved by using a variety of techniques in antenna systems. These include integrating RF-switches [46], loading the structure with external components to modulate the impedance [47], and employing tunable materials [48], Here, the author is exploring a fairly new concept with the SIW structures for the first time known as Field Programmable Microwave Substrate (FPMS) [18]

The concept of FPMS has been introduced by N. Jess [18] at Carleton University in 2016. However, the work mostly focused on the design of RF circuits rather than radiating elements. The heart of the idea is to modulate the substrate characteristics of a structure with the help of FPMS unit cells. By doing so, the designer can control the wave propagation through the designed component. The proof-of-concept of showed that tunable filters, programmable oscillators, and frequency-tuned amplifiers are all realizable using a single circuit board. The concept exhibits an unprecedented degree of programmability where not only the design is tunable but is also multifunctional thus opening a new door for the designs of smart RF components.

In this chapter, the principles of FPMS are covered by introducing the design and implementation of its unit cells. After providing a brief summary of [18], this section demonstrates how the FPMS unit cell dimensions and capacitance values are optimized for the slotted SIW design. All simulations are performed on a Duroid 5880 substrate with a 4 GHz central frequency, and the results are presented here.

## 3.1 Field Programmable Microwave Substrate

The operation of FPMS can be comprehended by first describing its building block, known as a "unit cell," and then describing its implementation to demonstrate its capabilities as a programmable waveguide [18].

### 3.1.1 FPMS Unit Cell

The individual unit cells utilized in the realization of FPMS can be exclusively reconfigured to have a range of positive or negative dielectric constants. It consists of two microstrip lines connected perpendicularly to one another. The intersection of the lines is loaded with a varactor diode that functions as a variable capacitor and is biased using an RF choke resistor, $R1$. The resistor operates for a larger frequency range which is an advantage over a conventional inductive choke. Parallel to this resistor is a capacitor $C1$ that acts as a DC blocker and provides an RF path to the ground. The design of the unit cell is depicted in Fig. 3.1. With it being the first-ever demonstration of the concept, the authors in [18] used FR4 as the substrate for practical purposes. Each unit cell consists of brown metallization, $V1$ varactor, $R1$ resistance of 10 $k\Omega$, and $C1$ decoupling capacitor of 2200 $pF$. Due to the fact that the metallization contains both direct-current (DC) and radio-frequency (RF) signals, resistance $R1$ and capacitance $C1$ are essential to the implementation of this structure. The optimized

unit cell design has dimensions of $W$ = 0.5 mm and $L$ = 2.54 mm, resulting in a plus shape metallization with total structural dimensions of 5.08 mm x 5.08 mm. FR4 board used in this work has a thickness of 1.17 mm with well-known dielectric characteristics of relative permittivity and loss tangent.

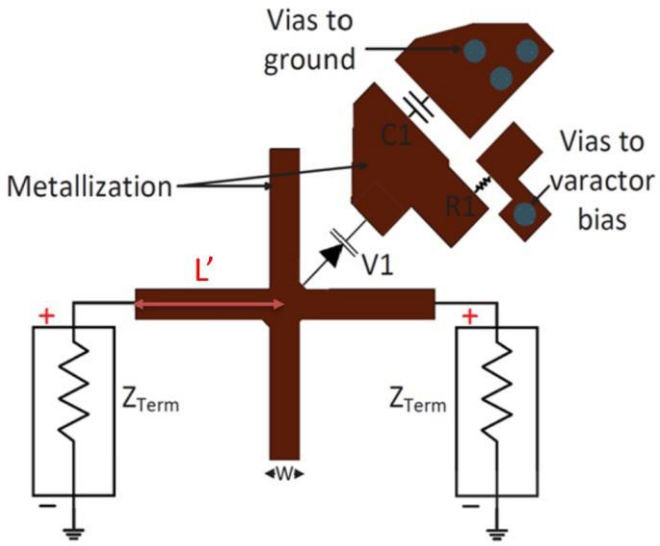


Figure 3.1: Unit cell used to construct FPMS [18]

Using Keysight's Advance Design System (ADS) in Momentum (layout) and co-simulation (EM and circuit simulation combined), the unit cell of Fig. 3.1 has been simulated [18]. The simulations are used to study the S-parameters of the two-port structure. These S-parameters can be used to extract the material properties experienced by the wave using Nicolson Ross-Weir (NRW) approach. The Nicolson-Ross-Weir (NRW) algorithm given in Equations 3.1-3.5 [49] is used to calculate the effective permittivity and permeability using s-parameters of the transmission line equivalent circuit.

$$\Gamma = \frac{S_{11}^2 - S_{21}^2 + 1}{2S_{11}} \pm \sqrt{\frac{S_{11}^2 - S_{21}^2 + 1^2}{2S_{11}} - 1} \tag{3.1}$$

$$T = \frac{S_{11} + S_{21} - \Gamma}{1 - (S_{11} + S_{21})\Gamma} \tag{3.2}$$

$$\frac{1}{\Lambda^2} = -[1/2\pi l\ (\ln 1/T) + i2\pi n] \tag{3.3}$$

$$\mu_r = \frac{1 + \Gamma}{(1 - \Gamma)\Lambda\sqrt{1/\lambda_o^2 - 1/\lambda_c^2}} \tag{3.4}$$

$$\varepsilon_r = \frac{\lambda_o^2}{\mu_r[1/\lambda_c^2 - 1/\Lambda^2]} \tag{3.5}$$

Where:

$\Gamma$ is the reflection coefficient

$T$ is the transmission coefficient.

$\mu_r$ is the relative permeability.

$\varepsilon_r$ is the relative permittivity.

$S_{11}$and $S_{21}$ are the reflection and transmission s-parameters.

$\lambda_o$ is the free-space wavelength.

$\lambda_c$ is the cut-off wavelength of the transmission line.

$l$ is the length of the sample and should be less than 180 electrical degrees.

$n$=0, $\pm$1, $\pm$2,…

By varying the bias on the varactor diode, the material properties of the structure can be controlled. The parameters illustrated in Fig. 3.2 demonstrate that the effective dielectric constant of the unit cell with the varying varactor bias. When the bias is changed from 25 V to 8 V, the dielectric constant fluctuates between 7 and 13 at 1 GHz. The reason for focusing on 1 GHz in this case is that 2 GHz is either very close to resonance or is the resonant frequency. Due to the limits of the FR-4 substrate,

which is only effective up to 4 GHz, and in order to keep the design simple, 1 to 2 GHz is chosen as the optimal frequency band for the implementation of the FPMS technology. It is also essential to note that the dielectric characteristics of the material at a specific bias remain constant until a maximum frequency known as the resonance frequency. This resonance point exists due to the resonance behavior of the unit cell which is dependent on the capacitance of the varactor diode and the inductive properties of the microstrip lines. By varying the capacitor value, one can control the resonant frequency of the FPMS unit cell. Once the resonance has been achieved, the wave experiences a negative permittivity as a result of the inverted reactance. These attributes are crucial because they determine the frequency bandwidth of the unit cell that can be tuned which will, in turn, control the frequency response of the RF component.

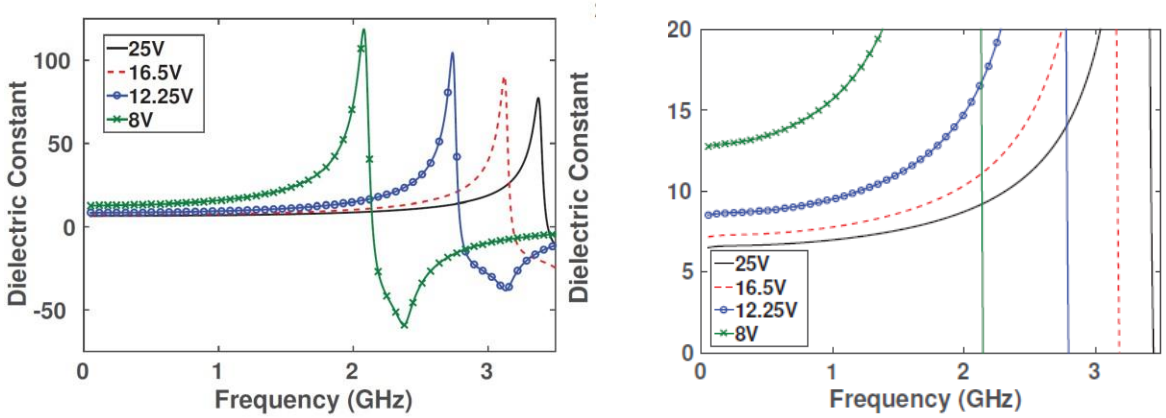


(a) (b)

Figure 3.2: (a) Effective dielectric constant of the unit cell (b) The magnified version [18]

In addition to the dielectric constant, the RF loss incurred by the EM wave is also studied. These results are added from [18] in Fig. 3.3. As expected, the resonance frequency in this instance is comparable to those shown in Fig. 3.2. It makes sense that the loss tangent values fall within the

range of 0.01-0.02 due to the use of FR-4 as the substrate. By using a lower loss substrate, one can deduce that these loss numbers can be further reduced.

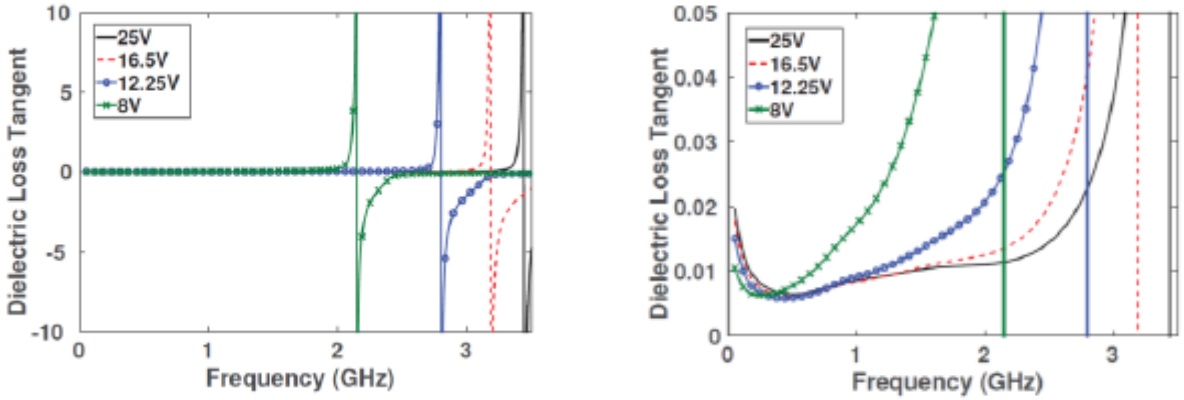


(a) (b)

Figure 3.3: (a) Effective dielectric loss tangent of the unit cell (b) The enlarged version of (a) [18]

In addition to the dielectric properties, the authors also studied the magnetic behavior of the unit cell, Fig. 3.4. In general, one would expect the relative magnetic constant of a substrate to be equal to 1 since it is non-magnetic in nature. Due to the increased series inductance from the metal cross structure used in the unit cell design, it is somewhat greater than 1 in this case. The magnetic loss tangent is also extracted and is shown here in Fig. 3.5. In an ideal situation (substrate), the material's magnetic loss should be zero due to the absence of magnetic dipoles. However, practically speaking this value would never be zero due to the losses incurred from other phenomena such as conductor loss. The sum of the magnetic and dielectric loss tangents results in the total power loss that a wave encounters when traveling through a medium.

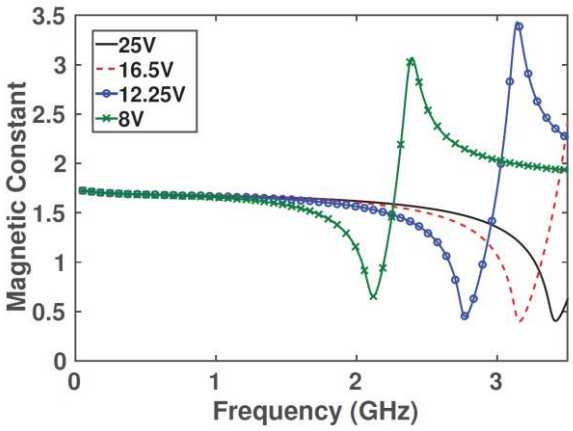


Figure 3.4 Effective magnetic constant of unit cell [18]

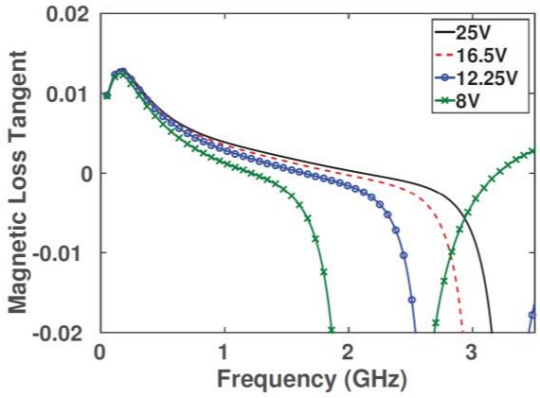


Figure 3.5: (a) Effective magnetic loss tangent of unit cell [18]

### 3.1.2 FPMS Implementation

With the introduction and analysis of the fundamental building block of FPMS technology, namely the unit cell, the next logical step is to apply its implementation in an actual PCB board and examine its effectiveness for the realization of fundamental RF/microwave components. Nathan *et al*. [18] designed and implemented a 16x16 element-based FPMS demonstration board using FR-4 substrate to accomplish this. The circuit board contains three microwave ports, a transistor with a common emitter configuration, an inductor (circle in red) that grounds the anode of the varactor, and two

capacitors (circle in blue) with a capacitance of 3pF to block DC and filter out low-frequency signals. Fig. 3.6(a) depicts the complete proof-of-concept design with a magnified version of the unit cells depicted in Fig. 3.6(b).

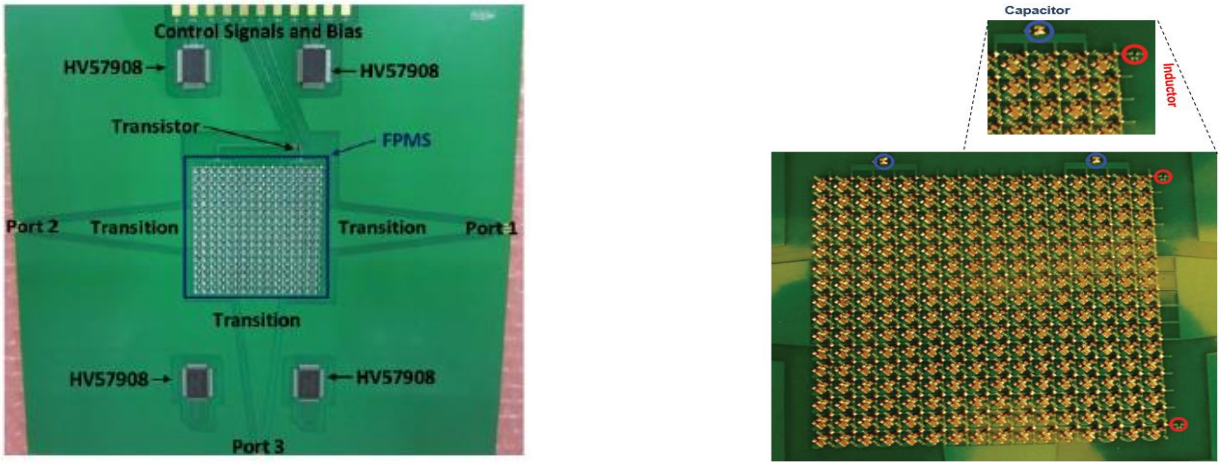


(a) (b)

Figure 3.6: (a) Implementation of FPMS on FR4 (b) Detailed image of an FPMS including 256-unit cells [18]

RF functions, including waveguide-based filters, oscillators, and amplifiers, are simulated and measured to confirm the integration of numerous functions on a single board. This level of adaptability is exclusive to the FPMS technology and exemplifies its originality. It is demonstrated that the waveguide may be tuned for its center frequency and impedance bandwidth with the help of the dynamic control provided by the FPMS unit cells to the designers. Similarly, the oscillator and amplifier functions are proven to be fully programmable by tuning the center frequency of these devices owing to the FPMS unit cells. For the sake of conciseness, only the results of waveguides are discussed in this chapter. The design is depicted in Fig 3.7, with each square block being realized using FPMS unit cells. These unit cells can be biased with varying varactor voltages to adjust the

dielectric characteristics experienced by the RF wave. In Fig. 3.7, the white blocks are biased to create a negative dielectric constant for the propagating wave, while the black blocks provide a positive dielectric constant. As a result, the wave only traverses the black sector, completely avoiding the white one. By selecting a variable number of black cells along the width, it is possible to change the waveguide's center frequency.

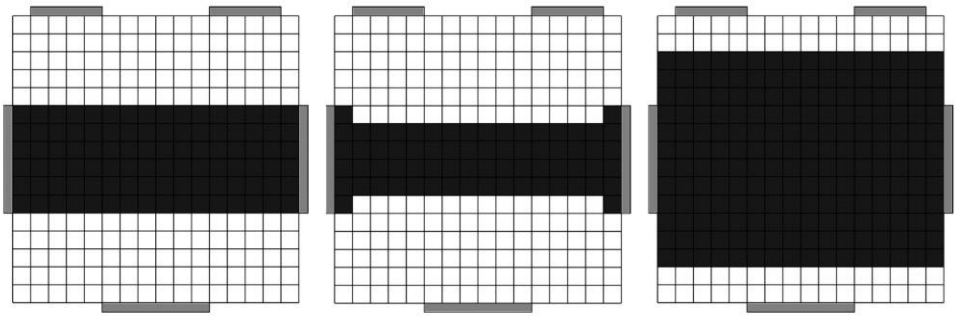

(a) (b) (c)

Figure 3.7: FPMS implementation for waveguide (a) Bias = 25 V. (b) Bias = 25 V. (c) Bias = 10.72 V [18]

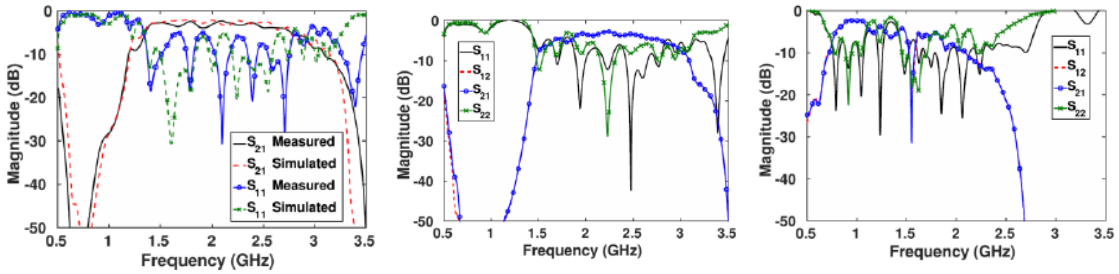


(a) (b) (c)

Figure 3.8: Simulated and experimental results (a) Bias = 25 V. (b) Bias = 25 V. (c) Bias = 10.72 V [18]

As seen in Fig. 3.8, the three waveguides with differing widths exhibit distinct frequency responses. According to the specifications, the impedance bandwidth and frequency can be altered with minimal effect on the insertion loss. In addition, it is demonstrated that the ON-voltage of the varactor can be altered to provide an additional degree of freedom. Therefore, both 25V and 10.7V are utilized in the test setup with minimal impact on performance.

## 3.2 Antenna Design Using FPMS technology

From the literature, it can be easily assessed that the novel technology of FPMS has been used only once for the design of an antenna [34]. Using a microstrip line based leaky wave antenna (MLWA), the authors showed how antenna radiation characteristics can be controlled using FPMS unit cells. By virtue of FPMS unit cells, the phase constant of the wave along the antenna length has been altered in a controlled fashion that in turn steers the maximum radiation of the beam. The proposed antenna structure is shown in Fig. 3.9 (a). The antenna provided a simulated gain of 11 dBi with a beam scanning range of ±30º at 2 GHz. Thus, the work of [34] has been used as a basis for the design work in this thesis.

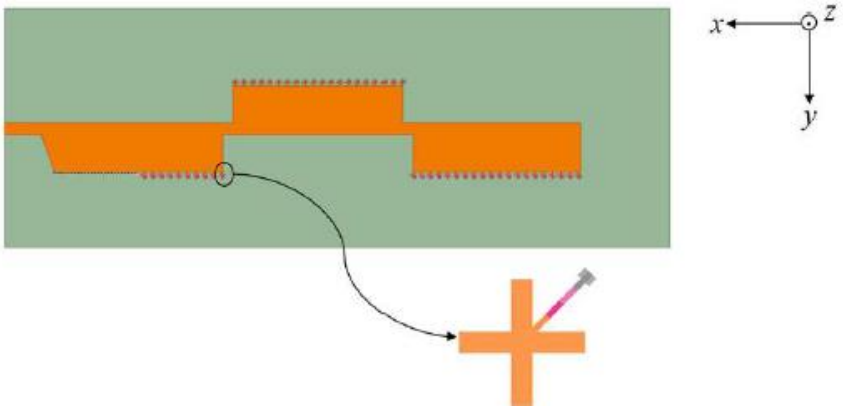


(a)

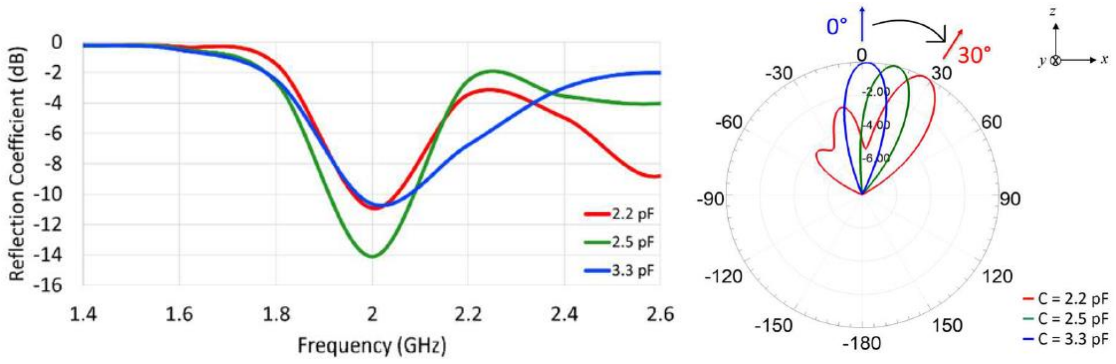


(b) (c)

Figure 3.9 (a) 2-D view of the proposed antenna design (b) S-parameters plot (c Plots of radiation patterns demonstrating beam steering

## 3.3 FPMS Unit Cell Optimization at 4 GHz

To design an antenna using FPMS unit cells, it is necessary to first understand their functioning principle using a Full-wave simulator such as Ansys High-Frequency Structure Simulator (HFSS). One of the goals of this thesis research is to investigate the employment of FPMS at higher frequency bands. Therefore, the design is intended to work at 4 GHz to target the application of military radars where beam steering is an essential requirement. FR-4 has been replaced with Duroid 5880 for this study due to the low loss and lower dielectric constant of the latter. The dimensions of the unit cell, substrate characteristics, and capacitance values are to be optimized to understand the operation of the unit cells as well as to study their integration with an antenna element. All of these variants are examined in-depth, and their discussion is included in the following sections.

### 3.3.1 Selection of the Substrate

Due to the presence of the antenna design using FPMS technology on the Duroid 5880 substrate [34], it is not required to authenticate the simulation model using Nathan's work [18]. Therefore, here the authors started the study of the unit cell using the details outlined in [34]. However, one key

difference between the antenna design of this thesis and the one reported in [34] is the difference in operating frequency. A change in the center frequency of 2 GHz may seem trivial at a quick glance, but it is well-known that this kind of change requires a new study to establish the basis for any design. Initially, a transmission line of length and width of 3mm and 0.5mm respectively, is simulated on a 1.575 mm thick Duroid 5880 substrate with a capacitor loading of 1pF. A dielectric constant of 2.2 and a loss tangent value of 0.0009 is used in the HFSS simulation environment to model the substrate. The resulting S-parameters from this unit cell are added in Fig. 3.10 (a). It is hard to extract any theoretical information from the S-parameter results themselves, rather it is important to use these simulations to generate the dielectric properties experienced by the RF wave using the NRW technique The extracted properties of the substrate are shown using in Fig. 3.10 (b). It is relatively easy to understand these results. It shows that the wave while traversing through the FPMS unit cell experiences a positive permittivity until ~3.5 GHz, the resonant frequency of the cell. Once the resonance point has been reached, the substrate exhibits negative permittivity to the wave. This means that the evanescence mode has been triggered and the wave cannot propagate normally through the medium.

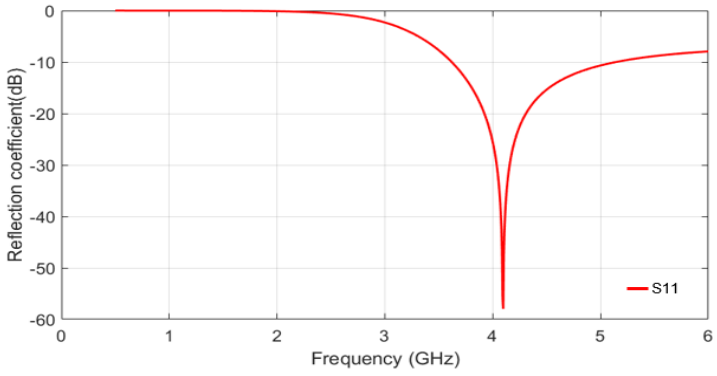


(a)

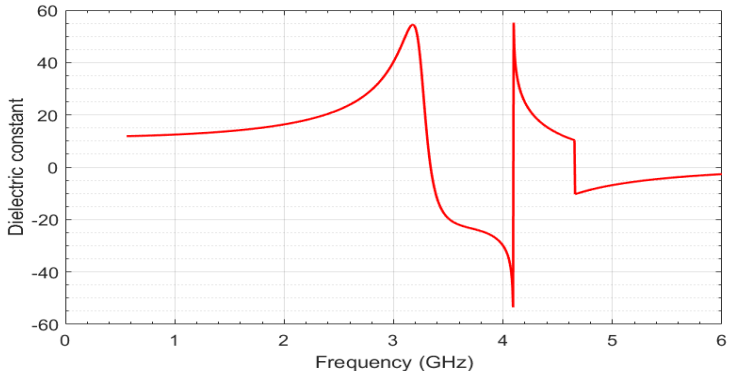


(b)

Figure 3.10: (a) Reflection Coefficient of the unit cell with dimension (3mm-by-0.5mm) on 1.575mm thick Duroid 5880 with capacitor loading of 1pF (b) Dielectric constant

These results are completely expected and are in line with the previously reported results of [18] and [34]. Using these results, one can now delve into further optimization of unit cell dimensions and the capacitor values to be integrated.

### 3.3.2 Optimization of the Unit Cell in Relation to Line Dimensions and Substrate Thickness

First, the unit cell should be studied for its performance by varying the length ($L$) of the metallization (orange) and the thickness ($T$) of the substrate, as depicted in Fig. 3.11. This major objective of these steps is to explore all available alternatives for the unit cell size and the influence of the substrate thickness on its impedance performance. The unit cell size should be practical in terms of both its implementation and frequency response. The width *'W'* of the metal is maintained at 0.5 mm since it does not play a significant role in varying the performance of the cell [18]. The lengths of the two metal lines are identical and are thus labeled as '$L$'. As indicated in Fig. 3.10, the capacitor is integrated at the junction of the two lines, again consistent with [18] and [34]. Since these are preliminary simulations, a capacitor with a fixed value (0.1pF) has been incorporated into the design

of the unit cell. Theoretically speaking, this is a low value and should result in a resonant frequency well above the operating frequency of 4 GHz. The length of the metal is the first variable considered in this investigation. First, the length of the metal is adjusted from 3 mm to 9 mm, while the thickness of the substrate is kept constant at 1.575 mm. This is the initial substrate thickness that may be used with Duroid 5880 and is commercially provided by the vendor. As mentioned previously that the unit cell is simulated using Ansys HFSS while MATLAB is used to retrieve the values of the dielectric constant from the simulated results. Also, when we were optimizing the unit cell, we keep our focus on two things, one is resonant frequency should not go too low then our target frequency which is 4GHz. So, we fix our target frequency and then very resonant frequency. Secondly, we also keep an eye on variation on permittivity, the more variation we get the more control we have over tunning the frequency. But our main focus is to keep resonant frequency over the target frequency. The collected findings are shown in Fig. 3.12.

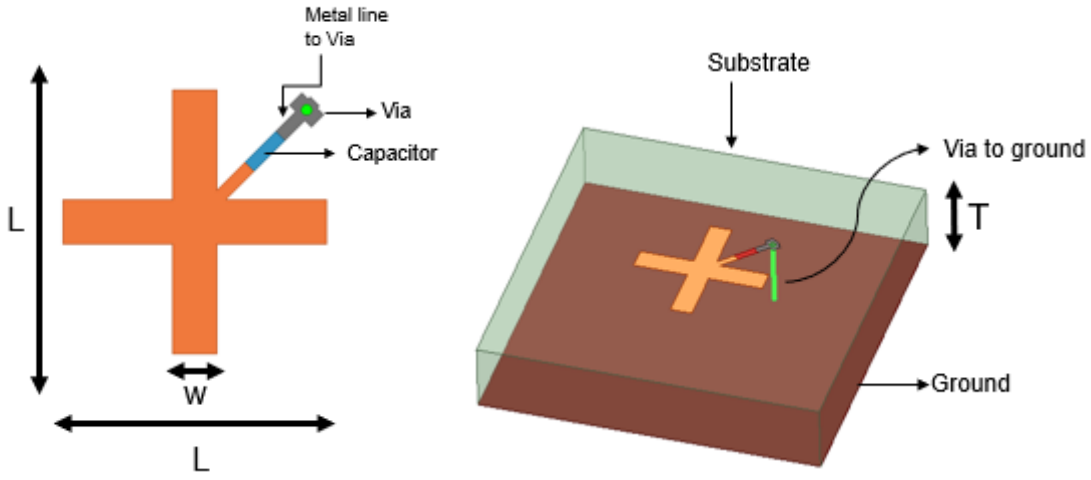


(a) (b)

Figure 3.11 Unit Cell under optimization (a) Top view (b) 3-D view

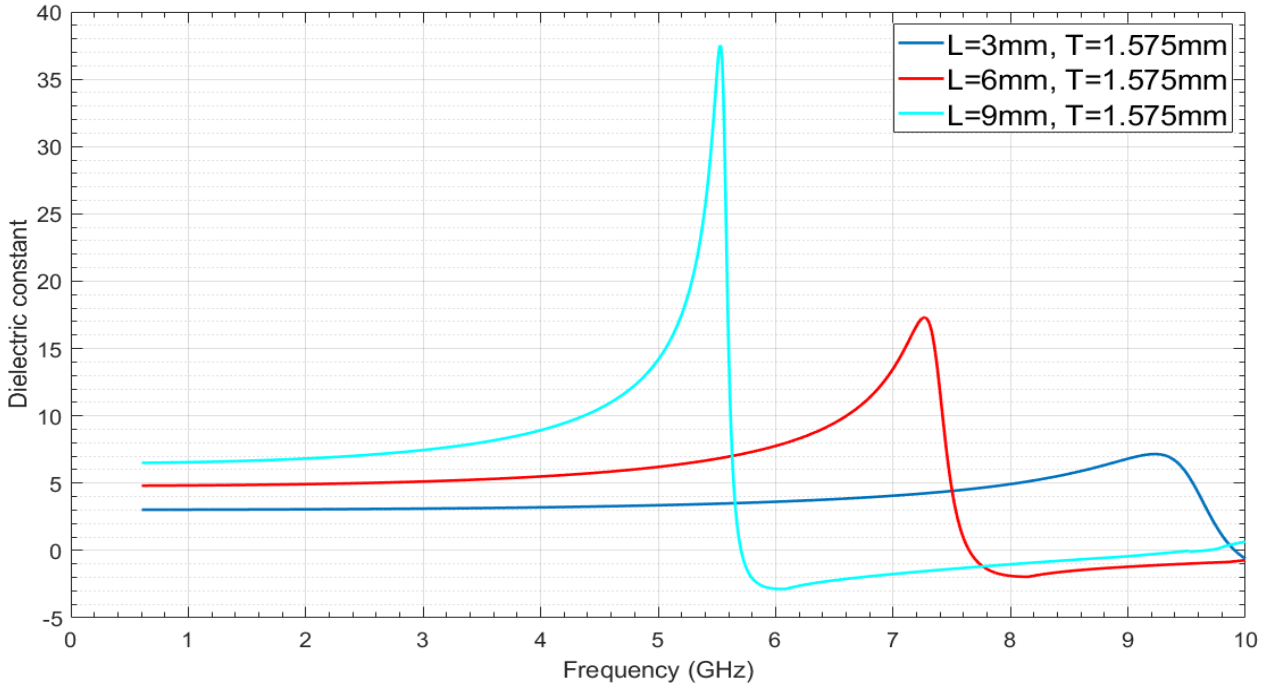


Figure 3.12: Simulated effective dielectric constant for change in *L* (3mm-9mm) while keeping the value of *T* at 1.575mm

In Fig. 3.12, when changing the length of the unit cell from 3 mm to 9 mm it is seen that the resonant frequency decreases while the dielectric constant value at frequencies below resonant frequency increases. This is an anticipated performance. As the length of the unit cell increases, the inductance offered by it to the wave also increases whereby the loading capacitor value is kept constant. This results in a decrease in the resonant frequency. At the same time, this phenomenon would cause the dielectric constant value to increase. Thus, these simulations are completely in accordance with Transmission Line Theory. In this instance, the desired frequency is 4 GHz, so the length value should keep the resonant frequency much above the desired center frequency. Based on this conclusion, $L = 3$ mm is an appropriate length for the lines as going below this number would cause the resonance to fall within the range of 4 GHz. However, this should be re-evaluated once the

substrate's thickness has been chosen as it may cause a change in this result. It is projected that increasing the substrate thickness would further reduce the resonance frequency. Therefore, staying slightly above 4 GHz is a safe practice here.

After evaluating the effect of changing the length of the lines, it is reasonable to analyze the effective change in the value of the substrate's dielectric constant caused due to the change in substrate thickness. For this aim, the thickness ($T$) of the substrate is altered from 1.575 mm to 4.75 mm, while the length ($L$) remained unchanged at 3 mm. The dielectric constant values derived from these simulations are shown in Fig. 3.13. The reason for using the specific thickness values shown in Fig. 3.13 is their commercial availability. Since the author is planning to eventually realize the antenna prototype, it is quite practical to use only these numbers.

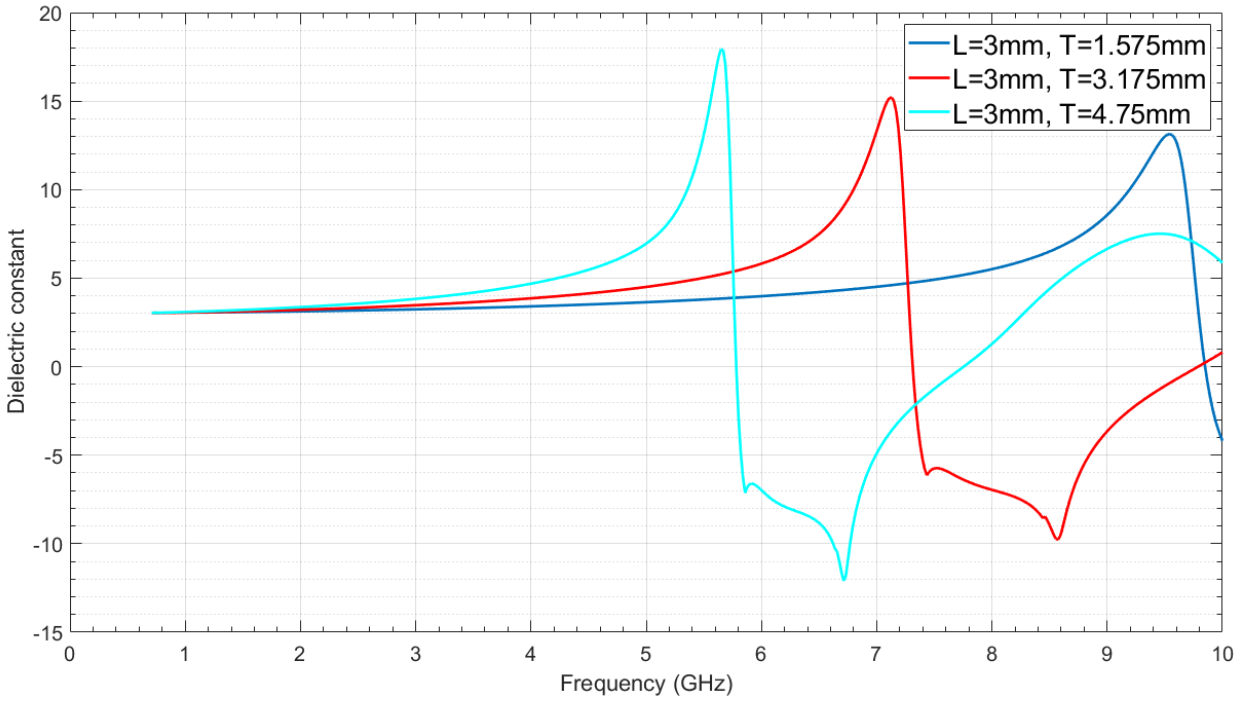


Figure 3.13: Simulated effective dielectric constant for change in T (1.575mm-4.75mm) while keeping $L$ at 3mm

The simulated findings displayed in Fig. 3.13 reveal that as thickness increases, the dielectric constant also increases. However, it is seen that the resonance frequency has an opposite trend meaning that it decreases with the increasing substrate thickness which is expected due to the increasing inductance of the via. For instance, at 4 GHz, the dielectric value for $L$ = 3 mm and T = 1.575 mm is observed to be 2.8, and when the substrate thickness increases to 4.75 mm, the dielectric constant value increases to 4.4. The simulation results are magnified in Fig. 3.14 so that the variation in the dielectric constant may be seen more clearly.

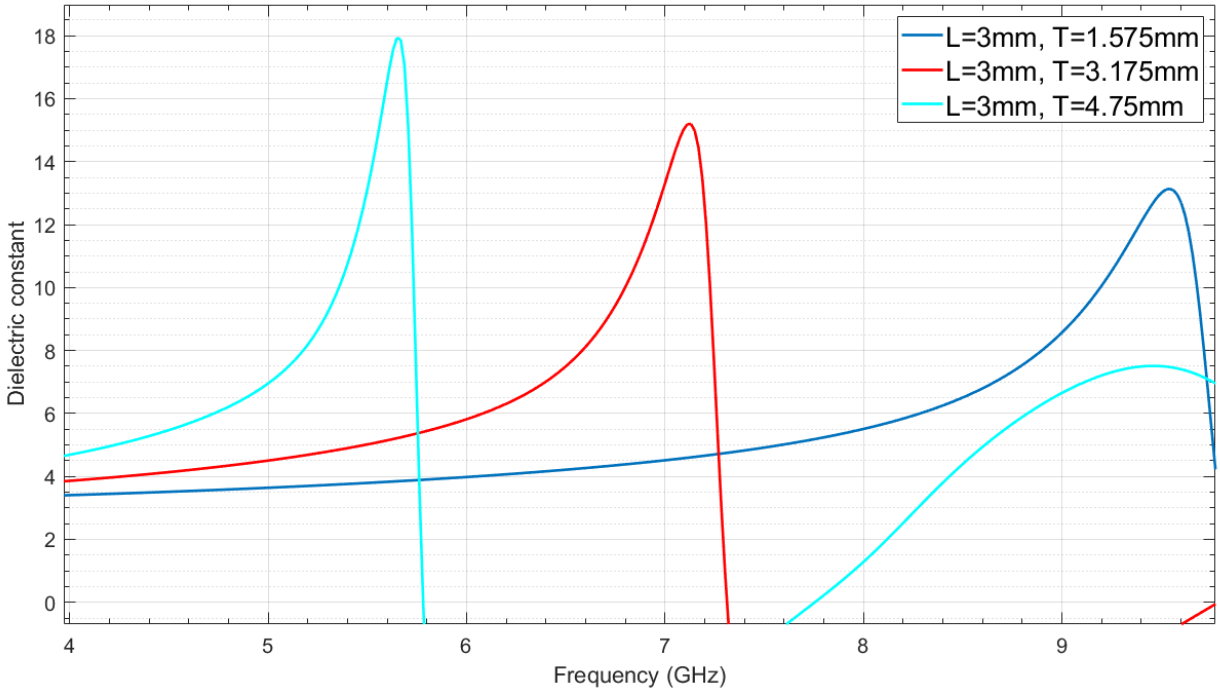


Figure 3.14: Magnified view of Fig. 3.13

For the final design, the plan is to integrate a large number of these unit cell structures directly onto the antenna. Therefore, the smaller these cells are, the simpler it is to integrate them with an RF component. Keeping this in view, the size ($L$) of the unit cell is chosen to be 3 mm-by 3mm on a substrate with a thickness ($T$) of 4.75 mm. It should be kept in mind that these values may change as

the antenna design is simulated on its own. However, with the results discussed in this chapter, it is easy to modify these numbers as per the desired performance requirements. Now, the next step is to see the effect of varying capacitance on the substrate properties.

### 3.3.3 Unit Cell Optimization with respect to Capacitance (C)

After analyzing the unit cell in terms of *L* and *T*, it is natural to look at the varying response with changing capacitance values. Using a via, the capacitor is added between the metal conductor line and the ground plane. The via represents an RF ground. In order to examine the influence of capacitance on the unit cell, the capacitance value is increased from 0.1 pF to 0.5 pF by taking resonance frequency into consideration. During the analysis of simulation data, the maximum limit on the resonant frequency is maintained at around 4.5 GHz, as it is in close proximity to the operating frequency. The variation in the dielectric constant is examined versus the changing capacitance value in Fig. 3.15.

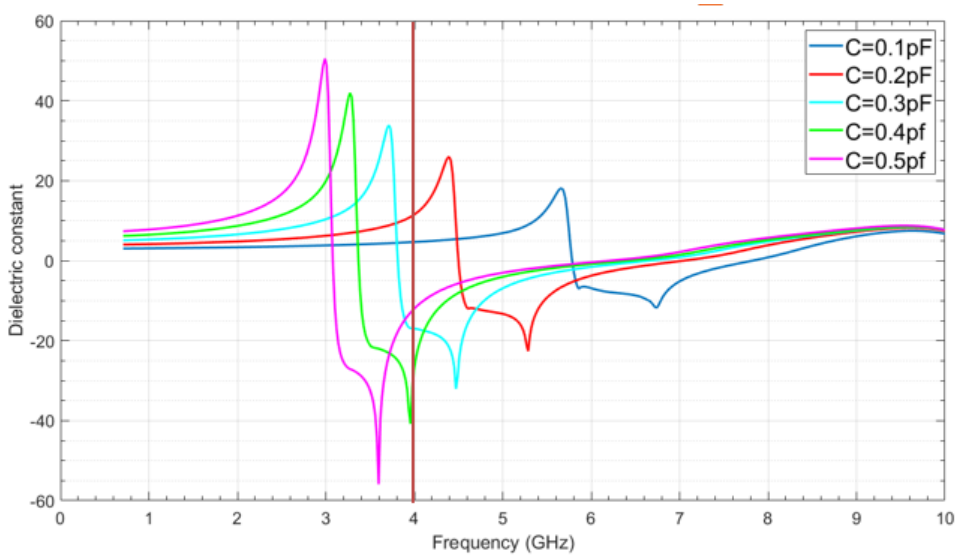


Figure 3.15: Change in dielectric and resonance frequency with change in capacitance

Again, the consequence of changing the capacitance value is rather interesting. As seen in Fig. 3.15, the resonance frequency is close to 4 GHz for a capacitance value of 0.2 pF. In addition, at the reference frequency of 4 GHz, the dielectric value is around 12 for 0.2 pF and increases as the value of the capacitor increases. Therefore, a maximum capacitance value of 0.2pF has been chosen for safety and to provide an acceptable dielectric constant range. Increasing the capacitance above 0.2 pF puts the unit cell's resonance frequency closer to the frequency of interest, namely 4 GHz. Since the antenna is to be loaded in an intelligent manner with the FPMS unit cell, it does not limit the designer to use only the positive dielectric constant values. Therefore, for now, it seems that the maximum range, in this case, is 0 to 0.2 pF, however, this can be only ascertained once the integration with the antenna is completed. This is a discussion for the next chapter and cannot be completed without knowing the antenna structure itself. For now, it can be stated that the unit cell simulated herein provides an acceptable range of performance for its use in the final antenna design.

## 3.3 Conclusion

A basic overview of FPMS and its unit cell has been covered in this chapter. After a thorough description of the unit cell's structure and how adjusting the bias voltages affects the dielectric properties, the unit cell has been tuned to operate at the desired frequency of 4 GHz. The process of optimization started with choosing the right material, which in this case is Duroid 5880. Once the substrate has been selected, the unit cell is studied for its varying dimensions and the values of the loaded capacitive element. With the resonant frequency of the unit cell in mind, an appropriate dimension of the structure has been selected that can be integrated with the antenna structure.

# Chapter 4

## FPMS-Based Slotted SIW Antenna

SIW-slot antennas belong to the family of antennas that are low-profile, low-loss, and simple to integrate with other planar circuits in order to achieve the desired radiating characteristics. However, it is evident from the preceding chapters that the emphasis of this thesis is on the design of reconfigurable antenna elements with a special focus on beam steering. For this purpose, a microstrip line-based antenna system is deemed to be most suitable for this work due to its compatibility with the novel FPMS technology. With the incorporation of FPMS unit cells into the antenna structure, a new SIW-slot antenna design is studied that can provide radiation pattern reconfigurability in the form of beam steering.

Initially, a slotted SIW presented in [16] is optimized in terms of its radiation performance so that it can operate at the frequency of interest i.e.,4 GHz. This is followed by the incorporation of FPMS unit cells into the antenna design. It is investigated how active FPMS unit cells may be used to modulate the antenna radiation. In this chapter, the radiation and impedance performance of the antenna are investigated, and the resulting findings are explained in detail.

## 4.1 Antenna Design from the Literature

This thesis examines the planar substrate integrated waveguide slot (SIW-slot) antenna described in [16]. The suggested antenna is realized on a single-layer substrate whose bottom layer is completely covered by a metal ground. However, this single antenna element is not capable of steering the antenna's maximum radiation on its own. Thus, the authors extended the design to a 1x8 planar

phased array system with integrated phase shifters to demonstrate the required beam steering. The design thus presented is capable of scanning the main beam on both sides of the elevation for the working frequency range of 5.4-6.45 GHz. The single element SIW slot antenna with a microstrip feed at its input is shown in Fig. 4.1 (a). It consists of 4 inclined slots that are etched longitudinally along the antenna structure. The slot is the active element of the SIW-slot antenna and offers the ideal impedance to the propagating wave, resulting in a specific radiation direction. Once integrated into the array system (Fig. 4.1 (b)), the authors showed how the main antenna beam can be controlled, Fig. 4.1 (c). The antenna's impedance performance is well within the acceptable range of performance. This is an interesting design with excellent antenna characteristics but like any other slot radiator, it relies on external phase shifters to get the desired beam steering. This design has been selected as the candidate for this work where the slots are to be treated as the main active element. It means that the FPMS unit cells are to be integrated into the slot structures to study their effect on the antenna radiation.

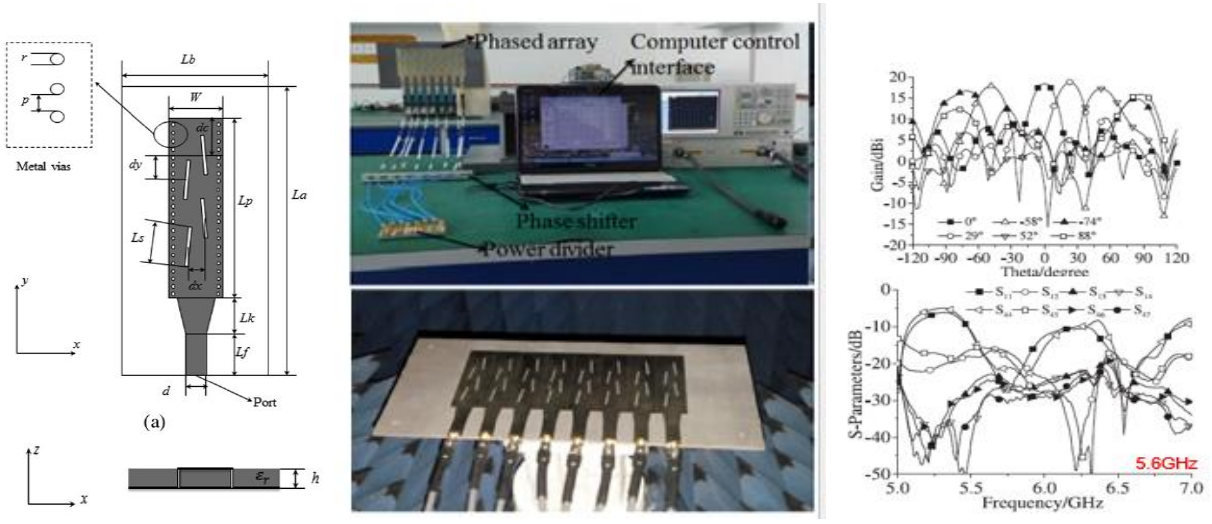


(a) (b) (c)

Figure 4.1 (a) Antenna under Study (b) Fabricated 1×8 phased (c) Radiation pattern and S-Parameter at 5.6GHz [16]

## 4.2 Optimization of SIW-Slot Antenna

After selecting the antenna under consideration, the next feasible step is to optimize the antenna design, first without FPMS unit cells tuned to the desired frequency. The optimization procedure begins with the implementation of the design in a full-wave simulator such as Ansys HFSS [38]. Initially, the antenna's dimensions stated in [16] are utilized to model the structure in the simulator on Duroid 5880 substrate (relative permittivity ($\varepsilon_r$)= 2.2, loss tangent (tanδ) = 0.0009). By properly selecting the simulation environment, the antenna's radiation properties are simulated and compared with the results presented in the published work. The conclusion is generally that the antenna performs well between 5.4-5.9 GHz as is reported. . In addition, it validates the simulation model that has been duplicated using HFSS and provides some assurance that any future results would be generally reliable. The reference antenna with its radiation pattern and reflection coefficient can be seen in Fig. 4.2. Both co-polarization and cross-polarization radiation patterns have been added here. After the design results have been replicated to a considerable extent, the actual designing phase of this task begins with optimizing the antenna to operate at the desired 4 GHz frequency.

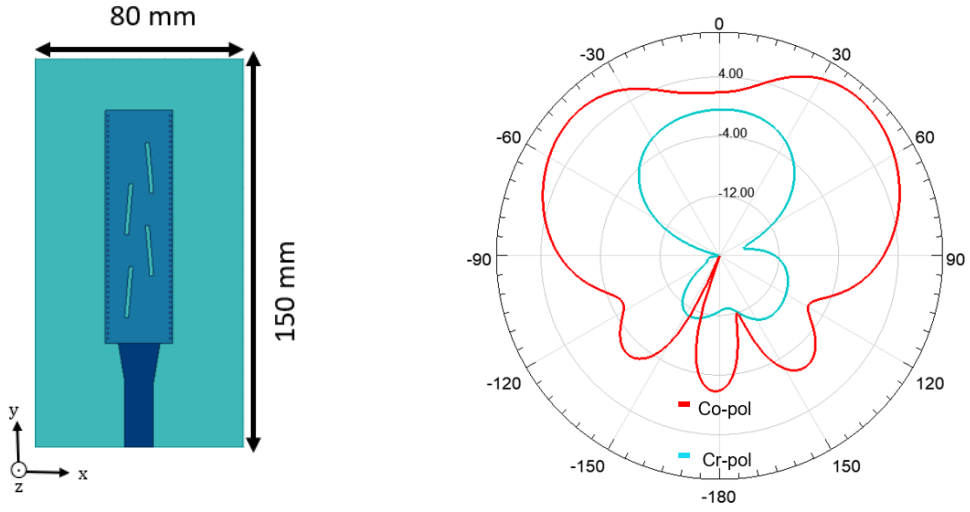


(a) (b)

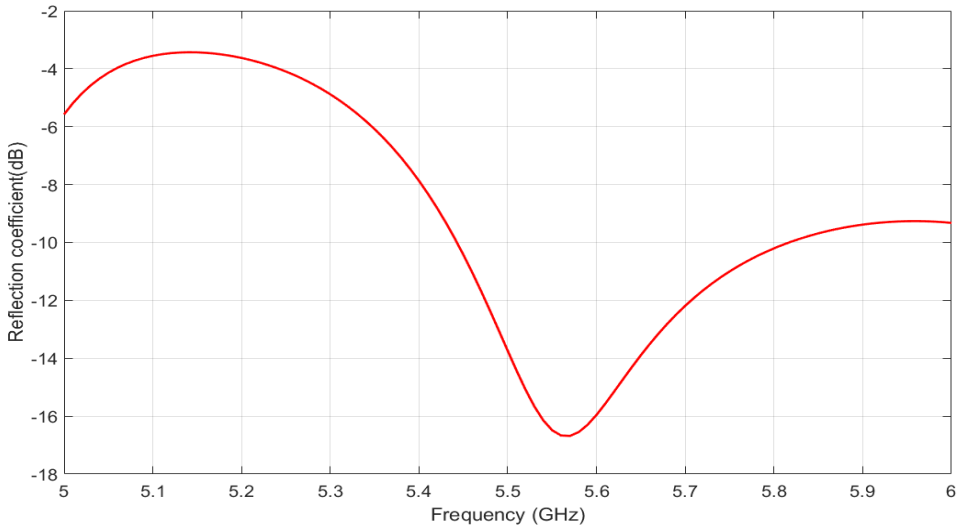


(c)

Figure 4.2 (a) Reference antenna (b) Radiation pattern at 5.6GHz (c) Simulated reflection coefficient

In order to optimize the antenna's operation at 4 GHz, different antenna dimensions are studied. At first, the number of slots is increased from 4 to 6 in hope of getting better gain and a narrower beam, a desired characteristic when steering the beam. is achieved. Each slot is inclined towards the center with an angle of 5º to the reference. This helps in matching the antenna; however, the slot cannot be rotated much due to poor radiation performance. Since, this part of the design has been extensively studied before, therefore in this design, the value of slot inclination is kept at 5°. As a result, the inclination is kept consistent with the original reported work. With a series of simulations on the slot placement and its dimensions, the design shows appropriate radiation performance with the slot dimensions of 24 mm x 3 mm. The antenna radiates well at 4 GHz with a maximum gain of 5.2 dBi. In addition, the antenna performance seems to be consistent with the original work which provides a certain degree of confidence in these simulations. The details of the antenna alongside its radiation performance at 4 GHz are added in Fig. 4.3 (a) and (b), respectively. Once these initial results have

been achieved, the next logical step is to integrate the FPMS unit cells that have been studied in chapter 3 of this document.

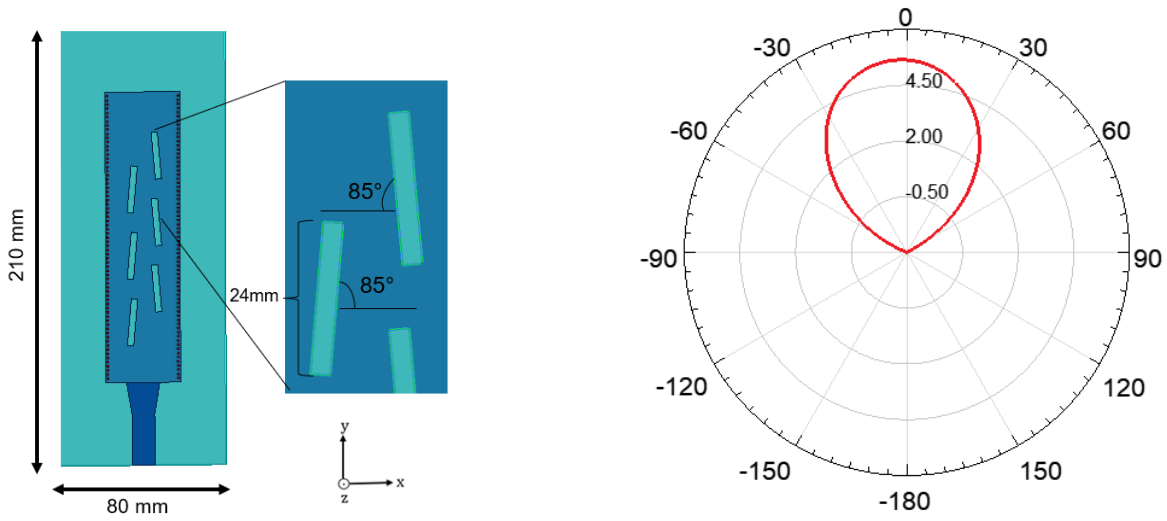


(a) (b)

Figure 4.3 (a) Optimized antenna without FPMS (b) Antenna radiation at 4 GHz with a gain of 5.2 dBi

## 4.3 Integration of FPMS to the SIW Antenna

SIW-based FPMS antenna design is completely absent from the literature. Therefore, without running some preliminary simulations it is hard to ascertain where the cells would perform the best. Thus, a variety of configurations are tried as a starting step to the antenna design. These configurations with the integrated unit cells are shown in Fig. 4.4. The unit cells are added in place of perfect electric conductor (PEC) via walls, in between the radiating slots, and around the slots themselves. With these integrations, almost no beam steering is observed from the antenna element.

This result is not completely unexpected. Since the slots are the main radiators in such a design, it can be safely assumed that major changes in the antenna performance are observed with the modifications in the slots themselves. However, it is important to study the effects of these unit cells around the radiating slots in order to validate the above statement. With this in mind, it is quite intuitive to add the FPMS unit cells right into the slot radiators.

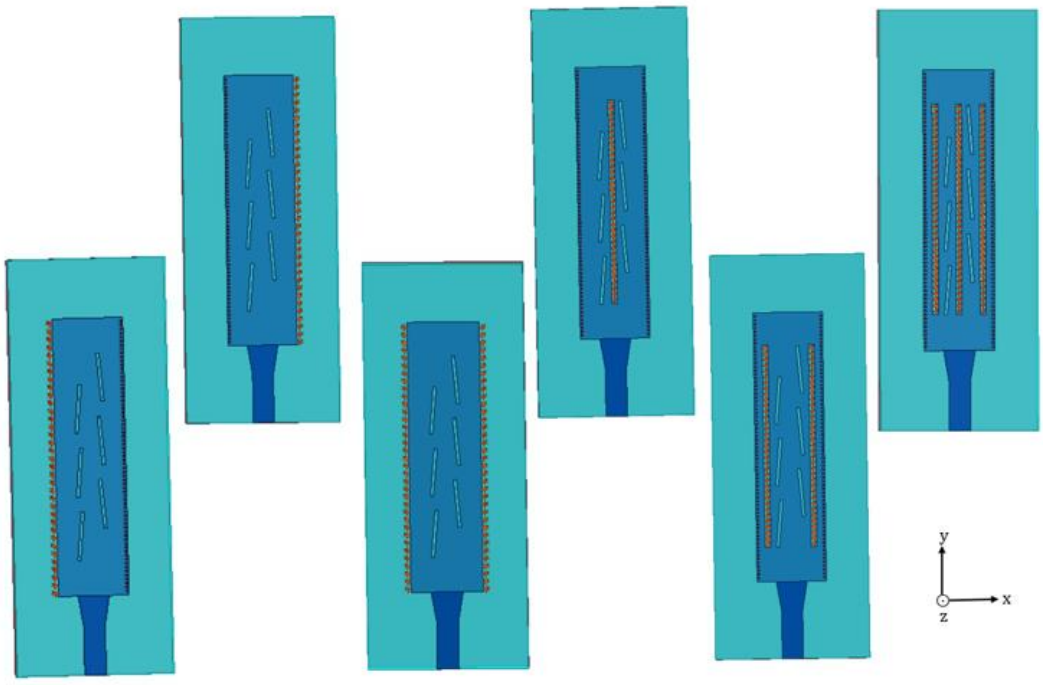


Figure 4.4: Different configurations of FPMS integration outside the antenna structure

The dimensions of the slot are such that it is easy to completely fill the space with a series of FPMS unit cells. The dimensions of a unit cell are 3 mm x 3 mm (chapter 2), whereas that of the antenna slots is 24 mm x 3 mm. It means that a linear array of 8 x 1-unit cells can be incorporated into each slot. This is deemed to be a good starting point for this study. When the antenna structure is simulated with this configuration, it is observed that the radiation is almost shorted. One rationale for this kind of response is the absence of the space for electric fields to resonate inside the antenna aperture. It is

well-known that a slot radiator emanates electromagnetic fields due to the presence of electric fields inside it that are attributed as magnetic current. If the slot cannot support such field patterns, then one cannot expect it to radiate well. Therefore, it is vital that some space is provided in the slot width to ensure some radiating fields or in other words to allow it to develop magnetic currents on it.

To achieve some radiations from the antenna, the slot width is increased from 3 mm to 4.5 mm. This kind of an arrangement would ensure some part of the slot to be free of metallic structures, thus resulting in some radiated fields. However, this means that the space around the unit cells can be arranged in different ways. For instance, in scenario 2, the FPMS unit cells are located on the left side of the slot (Fig.4.5(b)), while there is a 1.5mm gap on the right side of the slot, this is different from the design shown in Fig. 4.5 (a) where there is no space inside the slots after unit cell integration. The design in Fig. 4.5 (a) is the one that does not radiate well in the presence of the unit cells. Similarly, the FPMS unit cells are positioned on the right side of case 3 (Fig. 4.5(c)), whereas there is a 1.5 mm slot gap on the left. In addition, the side of the FPMS unit cells containing the vias is oriented toward the center of the antenna assembly. Similarly, instance 4 (Fig. 4.5 (d)) depicts a configuration in which FPMS unit cells are put in the middle of the slot, but there are 0.75mm gaps on either side of the slot. The width of the slots is maintained at 4.5mm, with the exception of case 2 (where it is 3 mm). 48 FPMS unit cells have been implemented in each of the four situations which means there are 8-unit cells in each slot. The use of 48-unit cells is necessitated by the size limitations of the slots. This is the maximum number of unit cells that can be added to the antenna construction given the dimensions of the slot and FPMS unit cell. Additionally, it is essential to note that the greater the number of unit cells, the better antenna properties may be controlled, however, this is an assertion at this point which would be verified with simulations. From the start, it is desired that

maximum controllability can be achieved. Therefore, the slots are integrated with as many unit cells as physically possible.

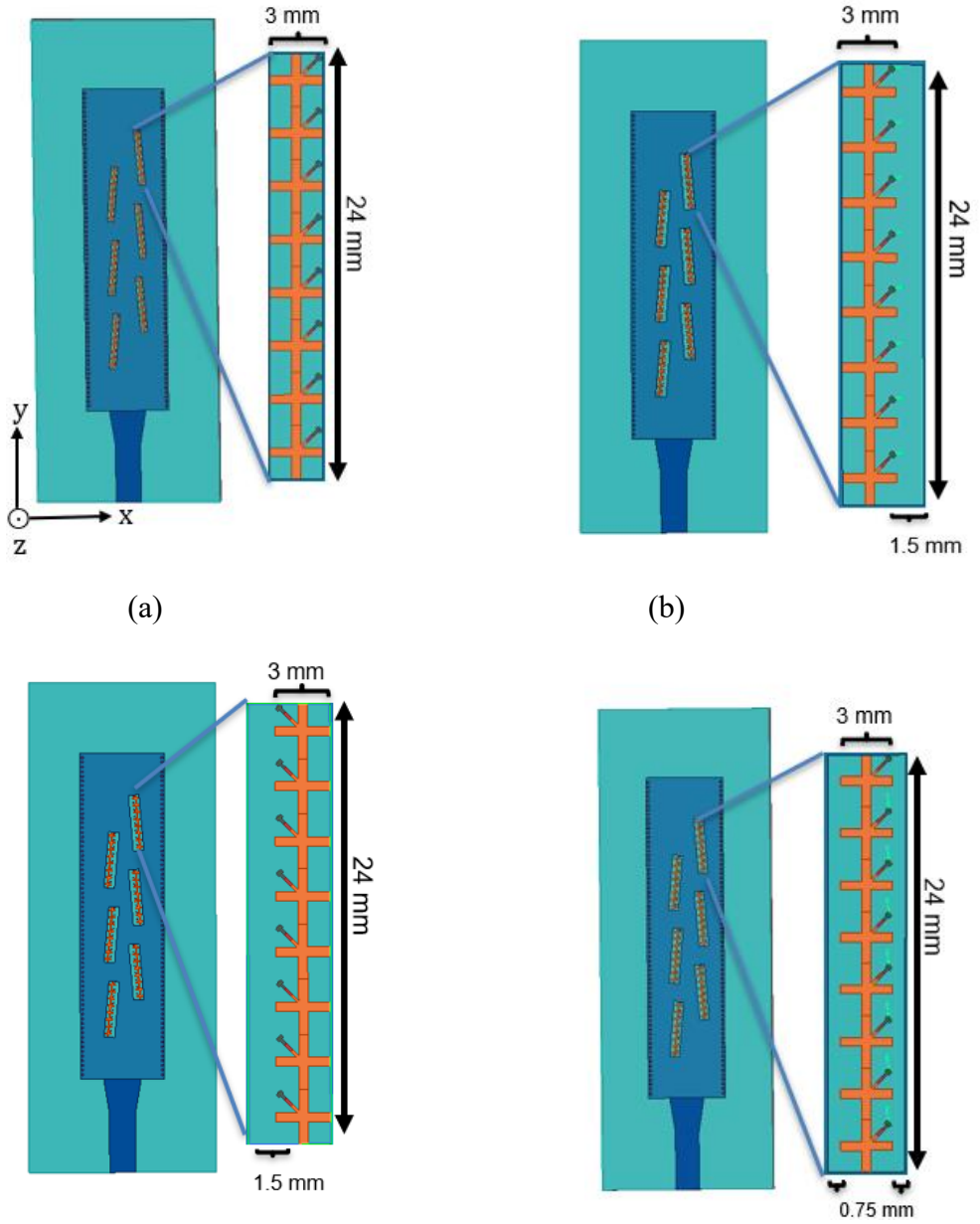


Figure 4.5: (a) Case 1: FPMS unit cell in the middle of the slot (without slot space) (b) Case 2: FPMS unit cell on the left side of the slot (c) Case 3: FPMS unit cell on the right side of the slot (d) Case 4: FPMS unit cell in the middle of the slot (with slot space on each side)

The simulation results for beam steering and reflection coefficient are investigated for each of the four antenna designs listed previously. In order to study the beam steering from these antennas, the capacitance of the unit cells is varied from 0.1 pF to 0.4 pF. These values are used keeping in view the results that are studied in chapter 3. Upon examining the results, it is evident that the integration of unit cells on the slots leads to beam steering, a favorable result. The best results among these designs are seen from case 3 (Fig. 4.5 (c)). A total of 42° of tilt is observed in the radiation and is shown in Fig. 4.6. The antenna seems to steer its radiation on the right side of the bore-sight radiation (0°) and therefore the angle of tilt is negative in Fig. 4.6. These results constitute the first step towards establishing the proof-of-concept for an FPMS-based SIW-slot antenna. To achieve the final results, however, additional optimization is needed.

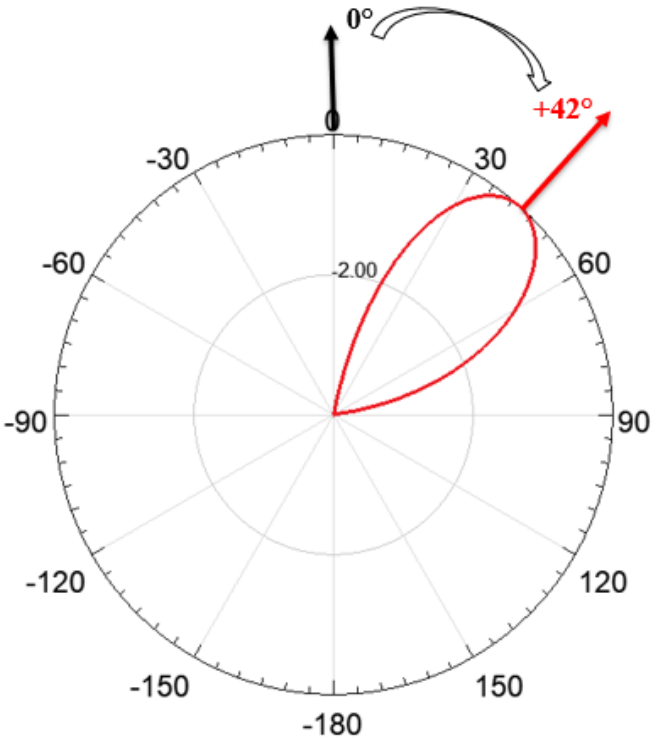


Figure 4.6: Normalized simulated radiation pattern of the proposed antenna with the capacitance of 0.2pF

### 4.3.1 FPMS Variable Capacitive Loading

There are a number of ways to test capacitive loading that should be discussed before moving on to the final results themselves. As discussed in the last sub-section that when varying the capacitance value of the unit cell, the maximum of the antenna does steer in one direction. At first, the capacitance of each slot is defined as '*C*' and varied to study its effects. This simulation setup is shown in Fig. 4.7 (a), however, this may not be the only configuration that can be employed here. In order to enhance the versatility of the design, it is imperative to study its performance when the slots are loaded with varying combinations of capacitance values. For example, in another case, the slots on the left side of the antenna length can be assigned one capacitance value, '*C*1', while the unit cells on the right side are to be loaded with a different value namely, '*C*2', Fig. 4.7 (b). Likewise, a different strategy where each slot has two different capacitances loaded onto the unit cells can also be studied for this design as shown in Fig. 4.7. (c). For the reader, it is obvious to extrapolate from here that there are a number of other scenarios that can be used to observe the antenna impedance and radiation characteristics. For this work, the study is limited to these 3 cases as they do result in the desired attributes of the antenna structure. An excellent advantage of this design is that with the help of varactor diodes and with one implementation, the designer can test various combinations in an actual scenario. Such a high level of reconfigurability is envisioned from FPMS technology and is being tested in such RF elements.

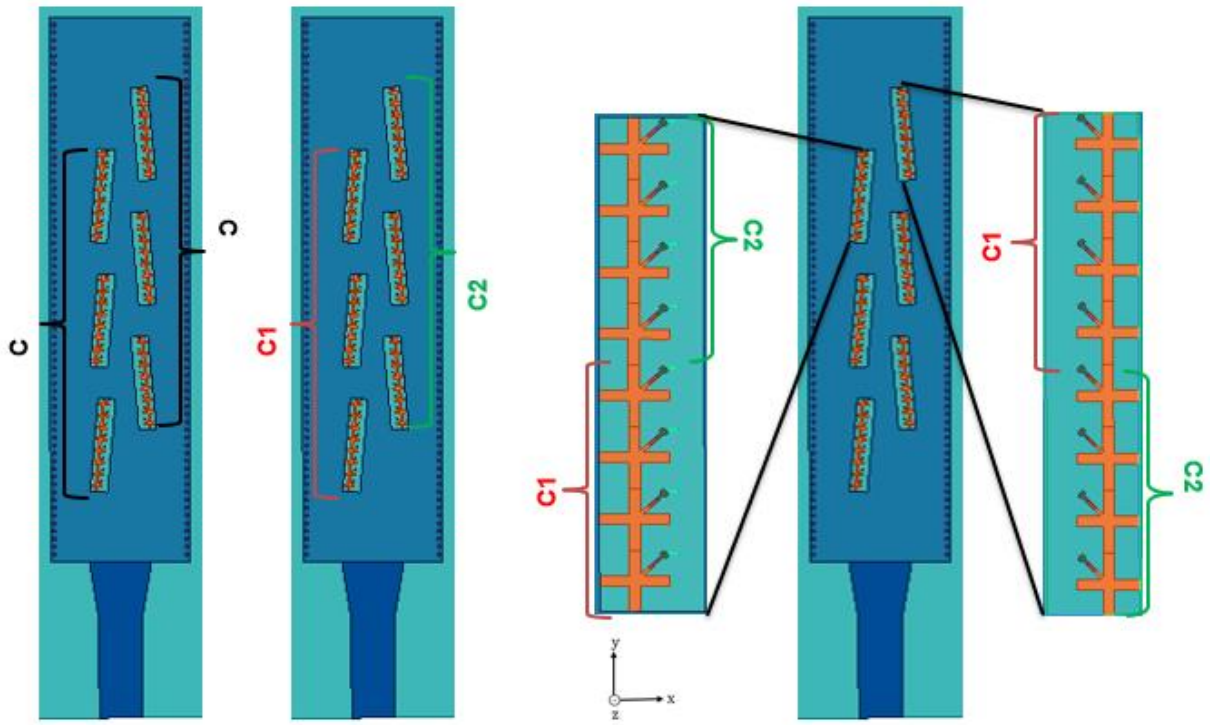


(a) (b) (c)

Figure 4.7: Different configurations for capacitive loading (a) Same capacitive values for all FPMS unit cells (b) Different capacitance values for left and right slots (c) Different capacitive values within each slot.

### 4.3.2 Beam Steering Radiation

Using a different combination of capacitances for the left and right array of slots, the antenna beam steering is observed. Initially, capacitance values of FPMS unit cells are varied from 0.1 pF to 0.4 pF in the HFSS simulation environment, Fig. 4.8 (a). As shown in Fig 4.8 (b), with $C$ = 0.2pF, the antenna is able to guide the radiation at +42º with a maximum gain of 5.6 dBi. As explained in the introduction of section 4.3, that initially the antenna is simulated with one capacitance value assigned to all unit cells. As a consequent step, the capacitance values on the two arrays of the slots are varied

independently. With the left side slots integrated with $C1$ and the right side using $C2$, the antenna is studied for its radiation properties, Fig. 4.9 (a). With $C1$ being 0.2 pF while $C2$ is kept at 0.1 pF, it is observed that the maximum radiation steers to -4°. This can be considered as radiation of the antenna to be in bore-sight (broadside) direction. The radiation pattern of the antenna for this particular configuration is shown in Fig. 4.9 (b). This is an interesting variation where the FPMS integration allows the antenna to steer its beam by ~40°.

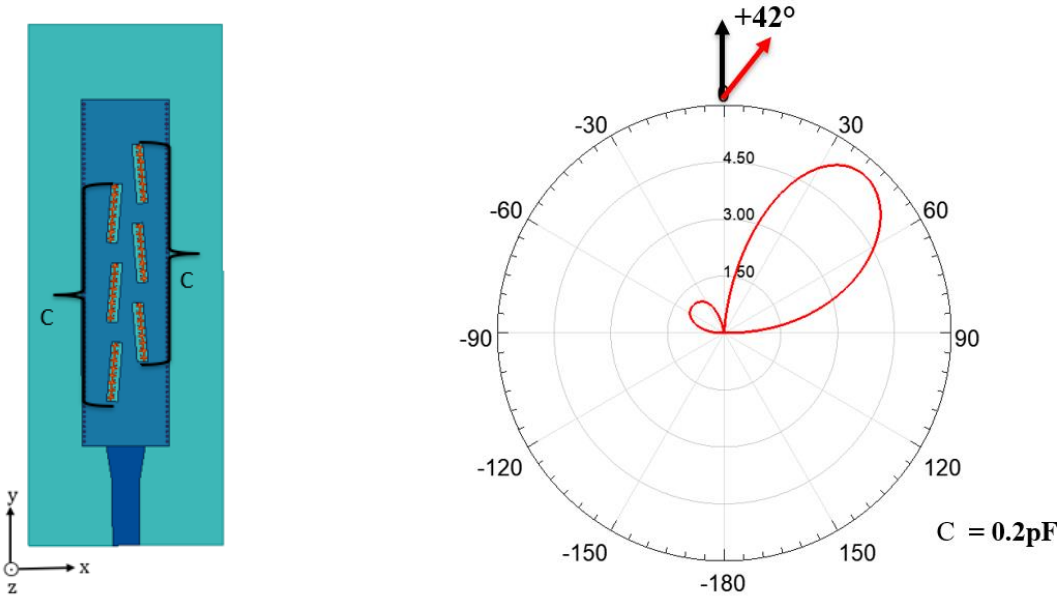


(a) (b)

Figure 4.8: (a) Corresponding antenna design with $C$ = 0.2 pF(b) Normalized radiation pattern

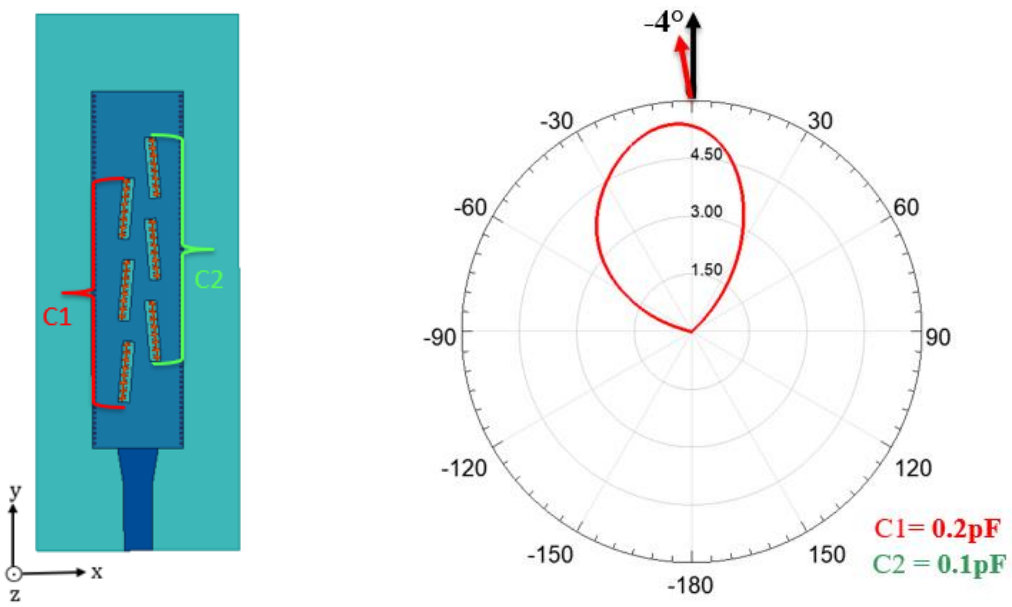


(a) (b)

Figure 4.9: (a) Corresponding antenna design with *C*1 *and C*2 (b) Normalized radiation pattern

As a next step, the author is interested in pursuing this further where the steering of the antenna beam can be extended beyond what is achieved in the last two iterations. For this purpose, *C*1 is kept at its original value of 0.1 pF while *C*2 is varied between over a range of 0.1 pF to 0.4 pF. The combination of *C*1 = 0.1 pF and *C*2 = 0.2pF resulted in the maximum radiation of 4 dBi at -42º as can be seen in Fig 4.10). It is also important to note that the beam steering angle of the main beam changed from -4° to -42°, which caused the amount of the side lobe radiation generated by the antenna to increase. The increase in the side lobe levels due to antenna steering is a known phenomenon. Generally, designers would like to steer the main beam until the side lobe level is at least 3 dB below the maximum value. The same criteria is maintained in this work. It is quite clear from Fig. 4.10 that the main beam of the normalized radiation is more than 3 dB above the side lobe of the antenna radiation. The three combinations of capacitance values discussed in this section allow the antenna to radiate

from -42° to 42°, however, these results are discrete in the sense that only three particular directions have been achieved. In order to claim that the design can actually provide continuous steering, it is imperative that the values between the two extremes of radiation are also achieved from the antenna structure. The simulations of the antenna that are furthered here do actually prove that the antenna can provide continuous steering. It can be seen from Fig. 4.11 that for the values listed in there, the antenna can actually cover the whole range. Thus, establishing that the design proposed here can provide continuous steering within the range prescribed above.

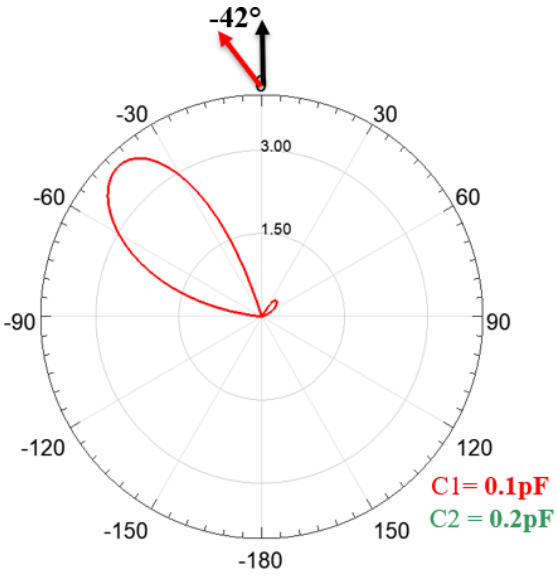


Figure 4.10: Normalized radiation pattern for corresponding antenna design with *C*1 *and C*2

A maximum gain variation of 2 dB is observed when the beam steers from -42° to 42°. With a simulated gain value of >5dBi, this variation is generally acceptable. The antenna may be able to provide better steering with some other values of capacitance, however, with a variation of 2 dB in gain and side lobe level reaching the main antenna gain, it is not prudent to scan the beam any further. Thus, these results can be regarded as an effective illustration of good beam scanning from a SIW-slot antenna with integrated FPMS unit cells. Also, a quick summary has been shown in Table 4.1.

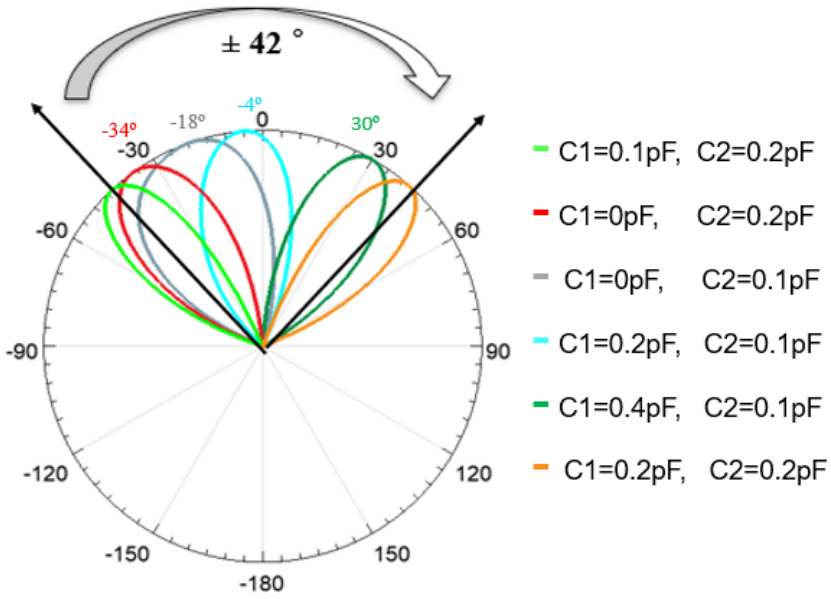


Figure 4.11: Normalized radiation pattern showing a beam steering of ±42º

Table 4.1: An overview of the beam steering angles and their corresponding capacitance and gain

| | **-42°** | **-34°** | **-18°** | **-4°** | **30°** | **42°** |
|---|---|---|---|---|---|---|
| **C1 (pF)** | 0.1 | 0.0 | 0.0 | 0.2 | 0.4 | 0.2 |
| **C2 (pF)** | 0.2 | 0.2 | 0.1 | 0.1 | 0.1 | 0.2 |
| **Gain dBi** | 3.99 | 4.01 | 5.99 | 5.41 | 5.45 | 5.59 |

It is vital to note that this design works well in terms of the radiation characteristics of the antenna, but the impedance performance is not up to the mark. The antenna does not exhibit matched conditions for the iterative analysis discussed in this sub-section. Therefore, it is important that the antenna is properly matched for its impedance for the design to be complete. This part would be covered in the subsequent section.

## 4.4 Antenna Optimization for Impedance Matching

To achieve improved antenna impedance performance, some antenna design needs to be optimized further. Consequently, a new study is required to achieve the desired results from the antenna. To accomplish this task, some new changes are introduced in the antenna parameters. At first, the tapered feed structure that joins the SIW part of the antenna with the microstrip feed line is swept for a range of dimensions to obtain the best possible results. One needs to acknowledge the challenge here that any dimensions should give the best impedance results for different capacitance values or in other words for all the directions of radiations. Therefore, the parametrization of the design here is extraordinary to achieve the set goals. In addition to the tapered feed structure, the length and width of the antenna slots are also varied to make sure that it incurs minimum reflection at the input.

Finally, the overall size of the antenna and the number of FPMS unit cells are also investigated to see if the antenna's matching improves. With all these variations, some changes in the antenna radiation is also observed but the author kept a keen eye on the radiation performance while carrying out these parameterizations. The final optimized antenna design that provides good matching conditions is shown in Fig. 4.12. With a length of 190 mm and a width of 80 mm, the antenna can steer the main lobe of the radiation from -42° to +42°. This design has 42 FPMS unit cells in total, with 7 FPMS unit cells in each slot with a 1.5 mm slot gap on the left side and a 0.5mm slot gap on the top. Each slot measures 21.5 mm in length and 4.5 mm in width. A total of 63 vias are used to define the PEC wall of the SIW structure with each via having a radius of 0.5 mm and spacing between consecutive vias to be 1 mm. The new values of capacitance that generates the required beam steering are listed in Table 4.2. The antenna radiation is exactly similar to the one shown in Fig. 4.11 and is not added here to avoid repetition. The antenna impedance performance is shown in Fig. 4.13. The reflection coefficient for all three variations shows matched conditions for the antenna.

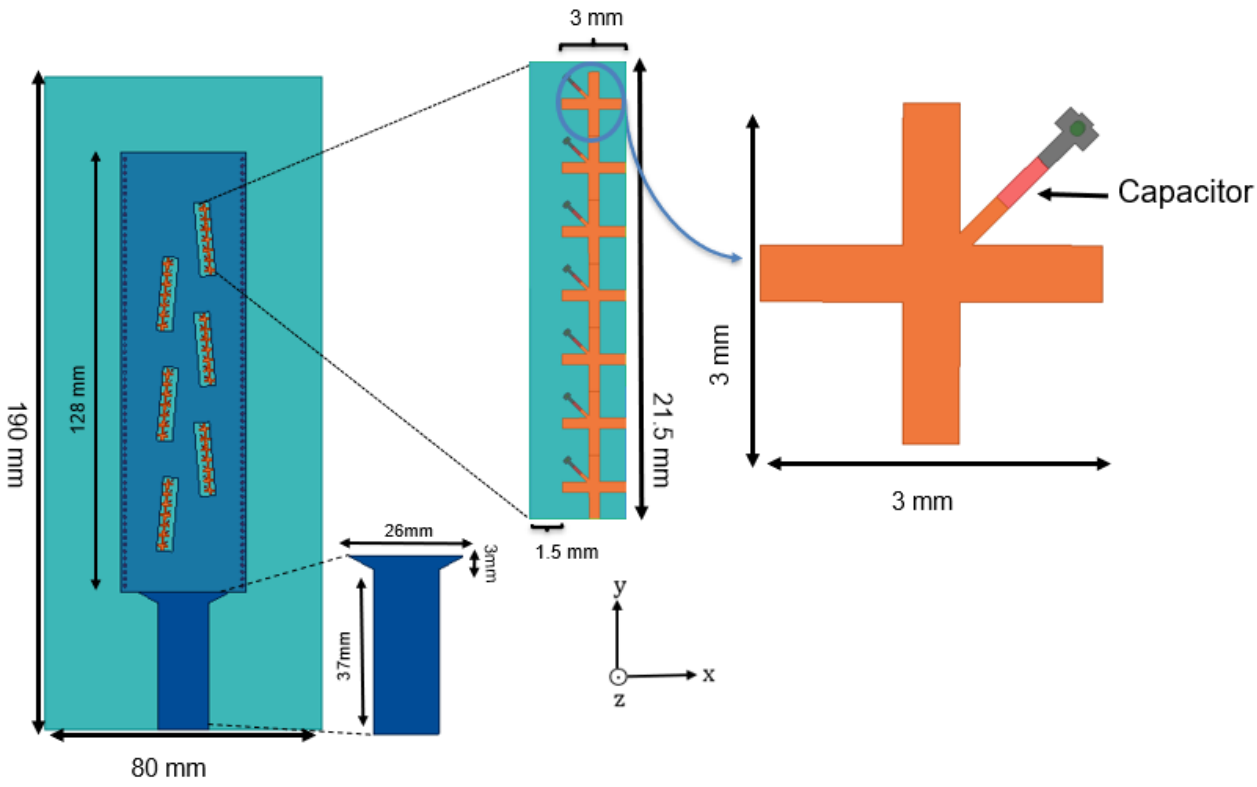


Figure 4.12: Final optimized design with FPMS unit cell

Table 4.2: An overview of the beam steering angles and their corresponding capacitance and gain

| | **-42°** | **-4°** | **42°** |
|---|---|---|---|
| **C1 (pF)** | 0.4 | 0.1 | 0.1 |
| **C2 (pF)** | 0.4 | 0.2 | 0.1 |
| **Gain dBi** | 6.11 | 4.08 | 5.59 |

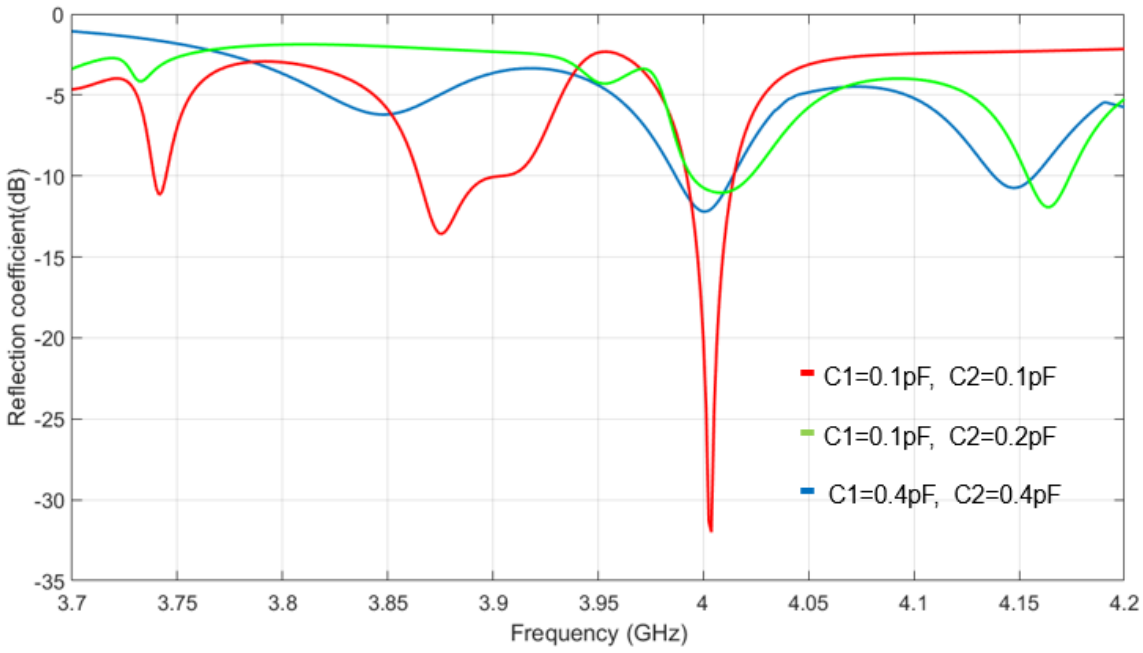


Figure 4.13: Reflection coefficient of the new antenna design to represent impedance response

With these results, it can be stated that the antenna provides good matching as well as radiation characteristics for the demonstration of beam steering. Thus, the design can be claimed as the first-ever SIW slot antenna realized using FPMS technology that can reconfigure antenna beam at a single frequency of operation.

## 4.5 Theoretical Explanation behind Beam steering

Although Ansys HFSS is a reliable industry-standard software that is used by antenna designers all over the world, it is still advantageous to grasp the physics behind things, as this can aid in developing a better knowledge of outcomes and to modify the design as per the needs. Therefore, in this section, it would be interesting to understand as to why the antenna behaves as a reconfigurable radiator when integrated with FPMS unit cells. At first, it is important to re-visit the operating principle of the SIW-

slot antenna. This will allow a better understanding of the FPMS integrated structure. In such a design, it is an established understanding that each slot operates as a radiator due to the presence of magnetic currents (or in other words the electric fields) on it. With the appropriate magnitude of the current and phase difference between the radiators, a principal beam is achieved from the antenna. A brief illustration of this hypothesis is provided in Fig. 4.14(a).

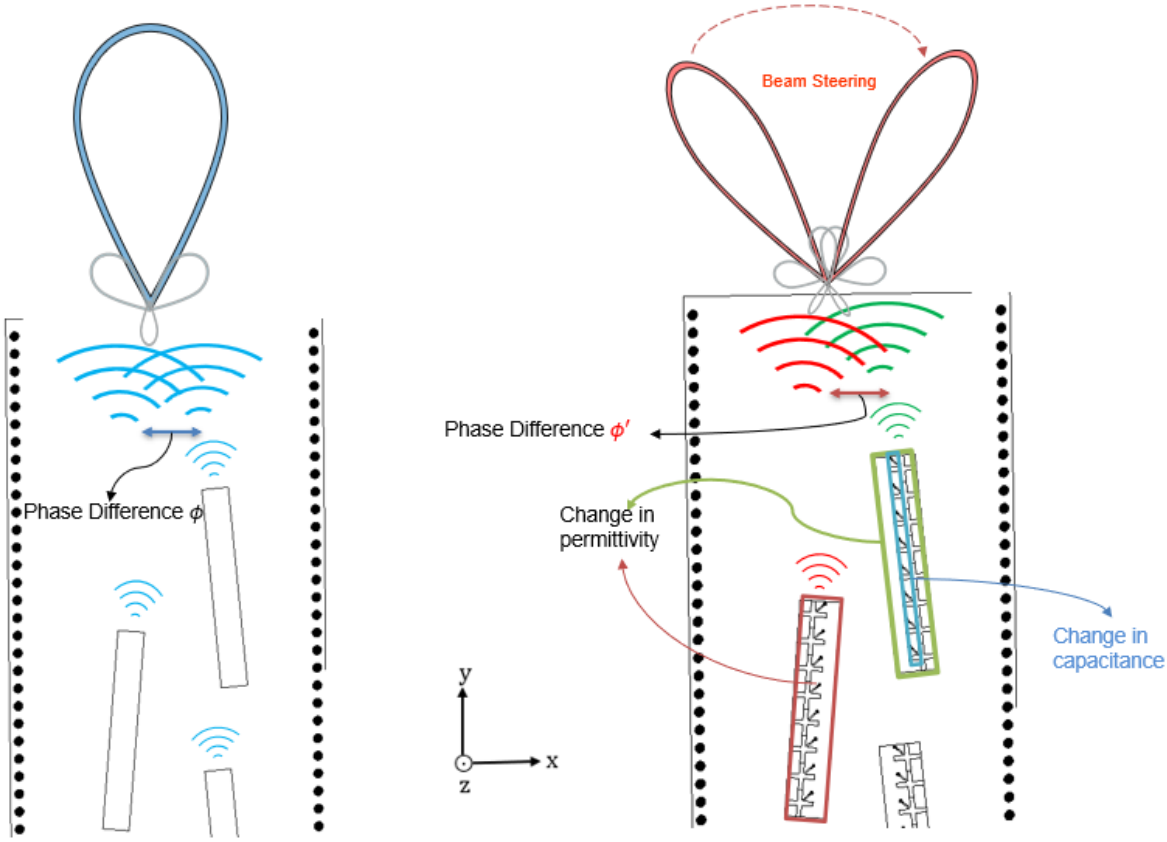


(a) (b)

Figure 4.14: (a) SIW-slot antenna without FPMS unit cells (b) SIW-slot antenna with FPMS unit cells

Now, when FPMS unit cells are integrated into the slots, the electric fields inside are perturbed and their values can be controlled with the help of the unit cell capacitance. The variation in capacitance

values is essentially changing the permittivity of the slots' edges. This variation in the permittivity/dielectric constant results in phase variations between the slot radiators. If the difference in phase changes differently depending on the scenario, the maximum radiation direction will shift. Using these FPMS unit cells, one can thus control the radiation from the antenna in a certain direction. It is important to reiterate here that by phase the author means the phase of the individual currents in the slots. This idea is illustrated pictorially in Fig 4.14 (b). This hypothesis has been validated by plotting the electric fields on the slot structures using Ansys HFSS.

## 4.6 Polarization Reconfigurability

Beam steering is one of the contributions of this thesis that has already been discussed in the last few sections. Another important aspect of the proposed antenna design is polarization reconfigurability. During the parametric sweeps of capacitance values, an interesting phenomenon is discovered in the antenna's radiation properties. The results indicate that the antenna radiates with θ-polarization at -42º and +42º (which means that $\boldsymbol{E}_\theta$ is the dominant component and $\boldsymbol{E}_\varphi$ is actually cross-polarization). However, as the antenna steers its beam from -42º to -4º, the radiation consists of both polarizations i.e., $\boldsymbol{E}_\theta$ and $\boldsymbol{E}_\varphi$ in the radiated fields. Eventually, as the direction of radiation reaches 0° (-4° to be precise), $\boldsymbol{E}_\varphi$ becomes the dominant polarization instead of $\boldsymbol{E}_\theta$. . This effect of polarization switching is plotted in Fig. 4.15. Following substantial research into polarization reconfigurability, it has been determined that the antenna polarization changes progressively from the maximum to the lowest direction. Table 4.2 includes a summary of gain values for the two normal electric field components for different directions of radiation. In the case of -42º $\boldsymbol{E}_\varphi$ is nearly 24 dB lower than $\boldsymbol{E}_\theta$, indicating pure $\boldsymbol{E}_\theta$ polarization of radiation, whereas in the case of -4º $\boldsymbol{E}_\theta$ is nearly 7 dB lower than $\boldsymbol{E}_\varphi$, indicating vice versa.

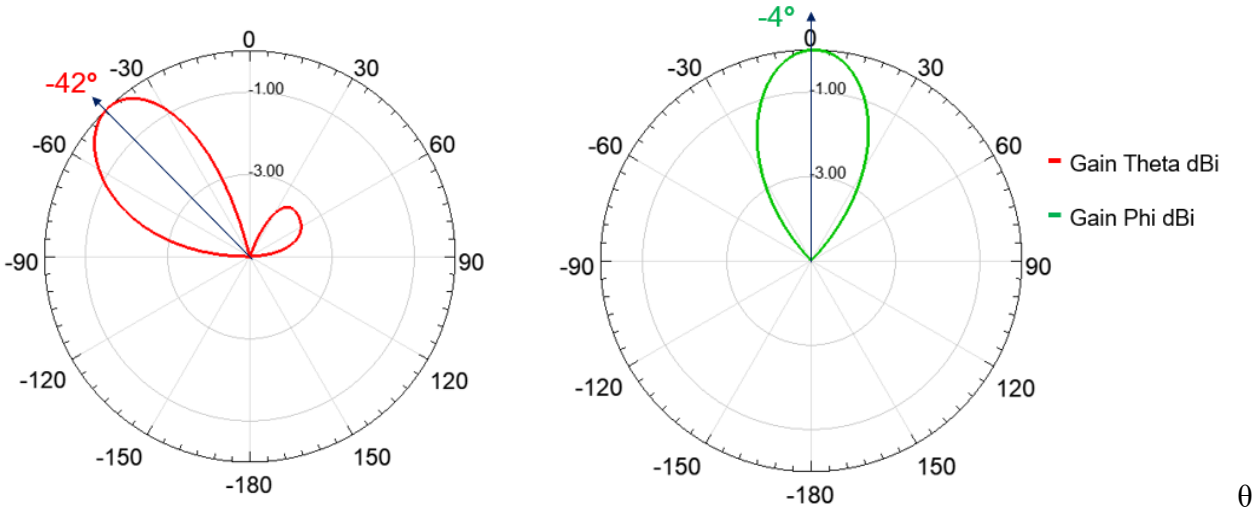


(a) (b)

Figure 4.15: (a) Gain θ radiation plot at -42º (b) Gain φ radiation plot at -4º

Table 4.2 A quick summary of Gain θ and ϕ together with their corresponding capacitance values.

| | **-42°** | **-4°** |
|---|---|---|
| **C1 (pF)** | 0.1 | 0.2 |
| **C2 (pF)** | 0.2 | 0.1 |
| **Gain Total dBi** | 3.99 | 5.41 |
| **Gain θ dBi** | 3.89 | -2.80 |
| **Gain ϕ dBi** | -19.88 | 4.45 |

Despite its limitations, polarization reconfigurability is extremely useful in secure point-to-point communication. For example, secure communication is used in the application of military radars and

communication. If the antenna on both the sending and receiving sides can change polarization, only the transmitter and receiver would know which polarization is required for communication. In this way, the communication cannot be infiltrated from external users. This is an interesting phenomenon that can provide its utilization in a variety of applications where security is of utmost importance.

Although it is an interesting characteristic of the antenna to switch its polarization when steering the antenna beam, one cannot leave it without paying attention to the reasons that result in such a performance especially because of its uniqueness. The resultant currents on the antenna structure are plotted using Ansys HFSS and observed closely. The directions of the currents are plotted in Fig. 4.16. To be clear, in this scenario, the overall result current is being mentioned, as opposed to individual slot currents that are discussed in the case of beam steering study. For the first case (Fig. 4.16 (a)), the current component is completely in the x-direction which is plotted for the case of $\varphi = 0°$. The conversion between the spherical and rectangular coordinates shows that in this case the x-component basically represents the θ-component of the vector. This is to say that the current here would result in far-field radiation that would be θ-polarized. Hence, the dominance of $\boldsymbol{E}_\theta$ over $\boldsymbol{E}_\varphi$ for this case of radiation.

Similarly, the φ-polarization is dominant in example 2 (Fig 4.16(b)), where the maximum radiation is at -4º. When the resultant current is plotted and inspected in this case, it is found that the component in the y-direction has a larger magnitude as compared to the one in the x-direction. Applying the same principles of coordinates conversion, it can be understood that this basically entails that $\boldsymbol{E}_\varphi$ component would be the dominant one in this case. A keen contrast between these two results is that in the first case the polarization of the antenna is completely θ-oriented with minimum cross-polarization levels whereas for the other case the cross-polarization levels are significantly higher,

and a pure φ-polarization is not achieved. Nevertheless, this is a unique property that is observed from the proposed antenna and one that is rarely seen in the existing literature. In the future, it would be interesting to study if further polarization diversity can be achieved using FPMS technology. For example, if it is possible to achieve two different polarizations in the same direction of radiation by controlling the capacitance values of the unit cells. These kinds of variations are an excellent candidate for the future study of such antenna structures.

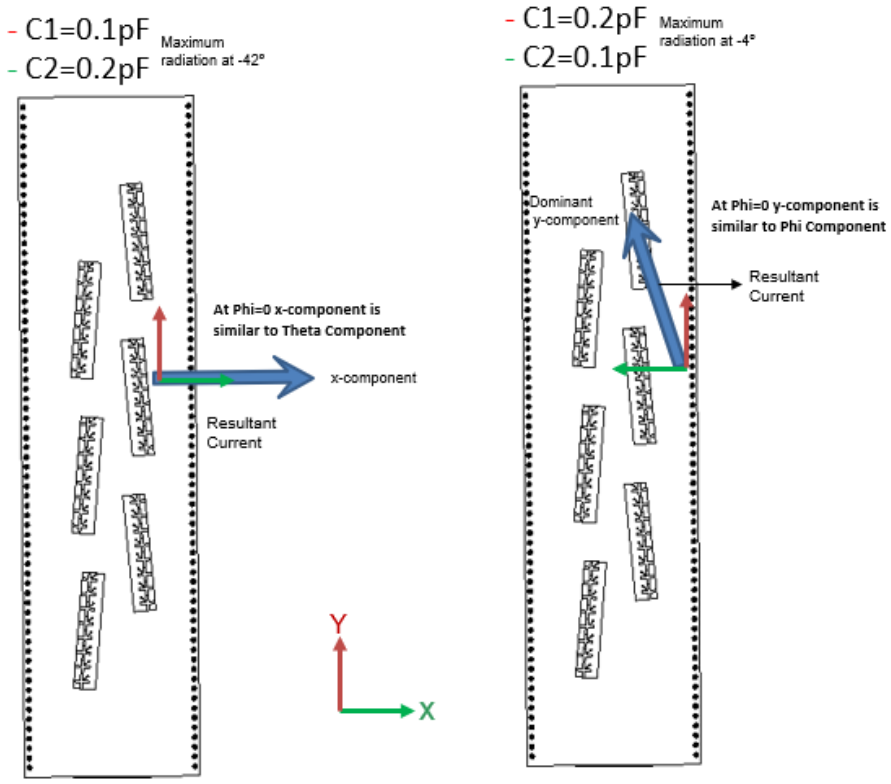


(a) (b)

Figure 4.16: (a) Total resultant current for theta polarization (b) Total resultant current in phi polarization

## 4.7 Gain Modulation

Gain modulation is another important contribution worth mentioning from the proposed antenna design. While studying the antenna reconfigurability, it is observed that for some directions of radiation, the maximum gain of the antenna can also be controlled. At a maximum radiation angle of -42º and a frequency of 4 GHz, a gain variation of 5 dB that translates into a linear value of 3.2 times has been attained, as shown in Fig 4.17.

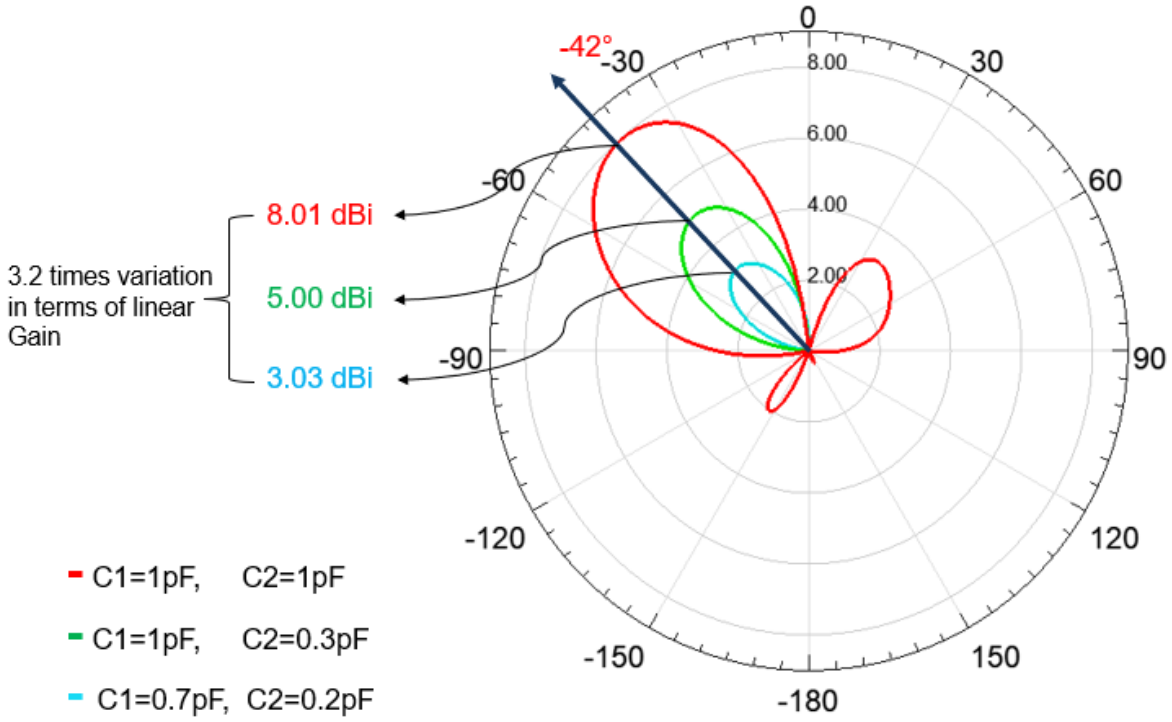


Figure 4.17: Radiation plots in dBi at 4GHz representing gain modulation at maximum radiation angle -42º

Theoretically, this phenomenon occurs when capacitance values are increased to the point where negative permittivity appears on the slots' edges. As a result, the electromagnetic field in the slot appears to be too concentrated mostly in the vacant space or the edge of the slot. This change in the current configuration would result in varying gain values since the magnitude of current dictates the

maximum gain emanating from an antenna. Since this phenomenon is not observed in all the radiating directions, one can say that this attribute from the antenna design is limited and cannot be employed generally. Having said that, this characteristic opens new avenues for research in gain-controlled antenna designs using FPMS technology.

## 4.8 Frequency Reconfigurability using FPMS

The level of adaptability introduced by FPMS in microwave components is unprecedented. Therefore, after investigating its use in the design of beam steerable antennas, it is pertinent to study its employment in achieving frequency reconfigurability. To accomplish this, a new strategy is used in the antenna design proposed in the last few sections. A group of FPMS unit cells are added at the input of the antenna just after the feeding structure, shown in Fig. 4.18. The rationale for this realization is the ability of FPMS unit cells to control the dielectric constant of the material. If one can intelligently control the properties of the substrate at the antenna's input, it may help in maneuvering the operating frequency of the antenna. Such a design provides more freedom to the designer while operating the antenna. Here only the capacitance values at the input are altered to study the impedance and radiation properties of the antenna while not changing the capacitances that are integrated inside the slots. The capacitances inside the slots are named as $C1$ and $C2$ (left-side slots as former and right-side slots as latter) while the unit cells at the input of the antenna are labeled as $C3$.

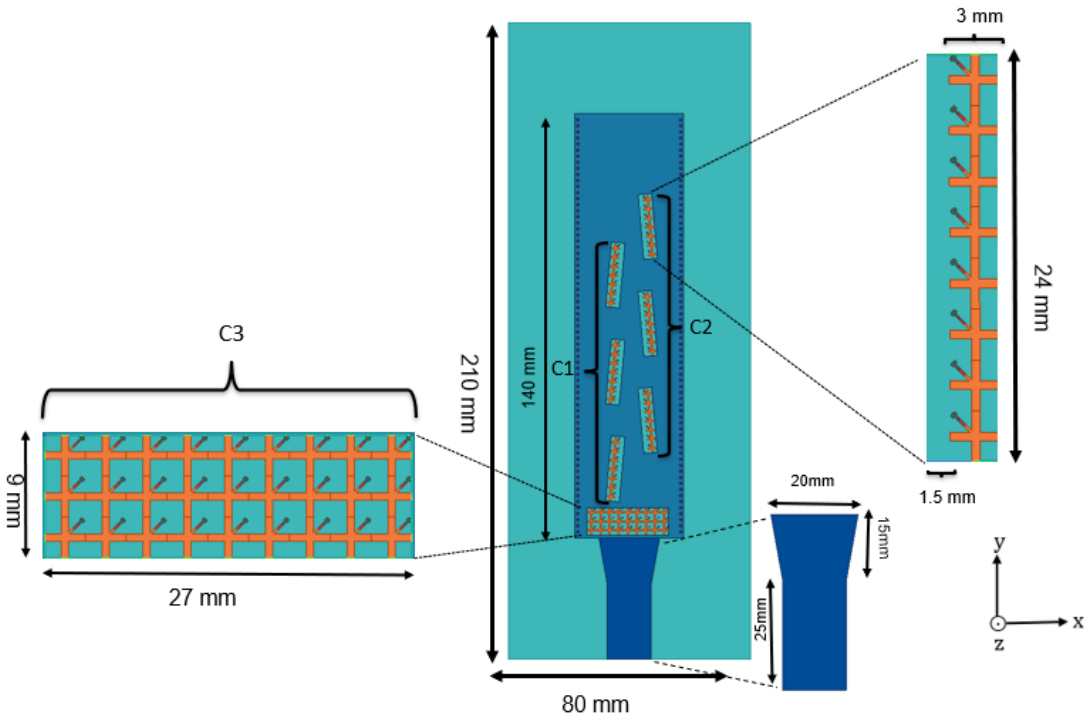


Figure 4.18: Final optimized design for frequency tunability

In order to investigate frequency tunability, a parametric analysis with different capacitance values *C*3 for the new slot with FPMS unit cells is performed. For the initial simulation, *C*3 is swept from 0.1 pF to 0.5 pF while keeping *C*1 and *C*2 equal to 0.1 pF. For the value of *C*3 equal to 0.1 pF, 0.2 pF, and 0.3 pF the antenna radiates at 4.1 GHz, 3.5 GHz, and 3 GHz, respectively as can be seen in Fig. 4.19. Based on the results, we can deduce that as the value of *C*3 is increased, the frequency decreases, hence providing the intended impedance tuning. For the most part, the gain of the antenna does not change much as the frequency tunes down. The values of the gain are added in Fig. 4.19 caption. In addition, the radiation pattern of the antenna changes slightly but in general, the antenna radiates in the bore-sight direction. The consistent gain and the radiation characteristics validate the frequency tunability of the proposed design. However, one needs to look into the impedance response also to validate the antenna performance. The reflection coefficient of the antenna for different values

of *C*3 are plotted in Fig. 4.20. The mismatch of the antenna for all three cases is almost negligible showing good matching conditions. These two results (Fig. 4.19 and 4.20) in tandem prove that the antenna structure proposed herewith provides frequency tunability while maintaining the radiation properties of the antenna.

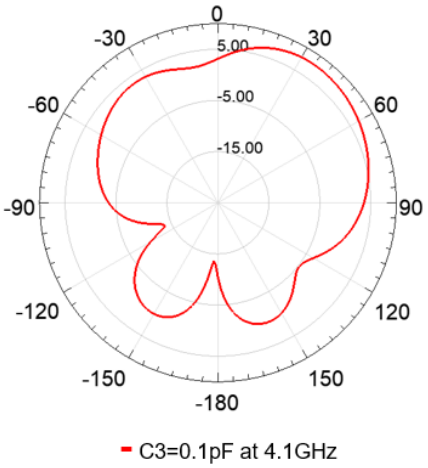


(a)

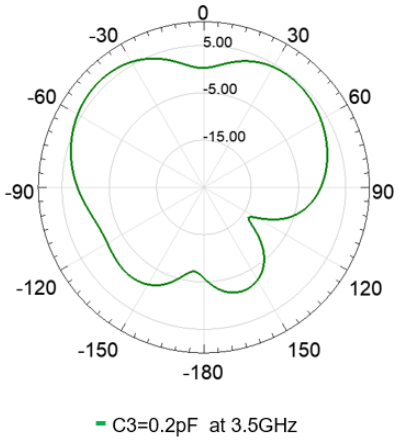


(b)

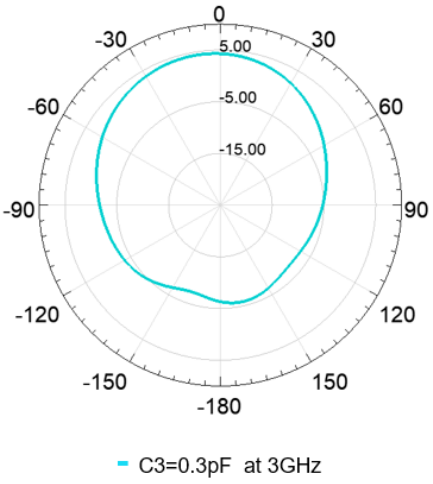


(c)

Figure 4.19: *x-z* plane radiation pattern in dB (a) 6.5 dBi at 4.1 GHz (b) 5.8 dBi at 3.5 GHz (c) 5 dBi at 3 GHz

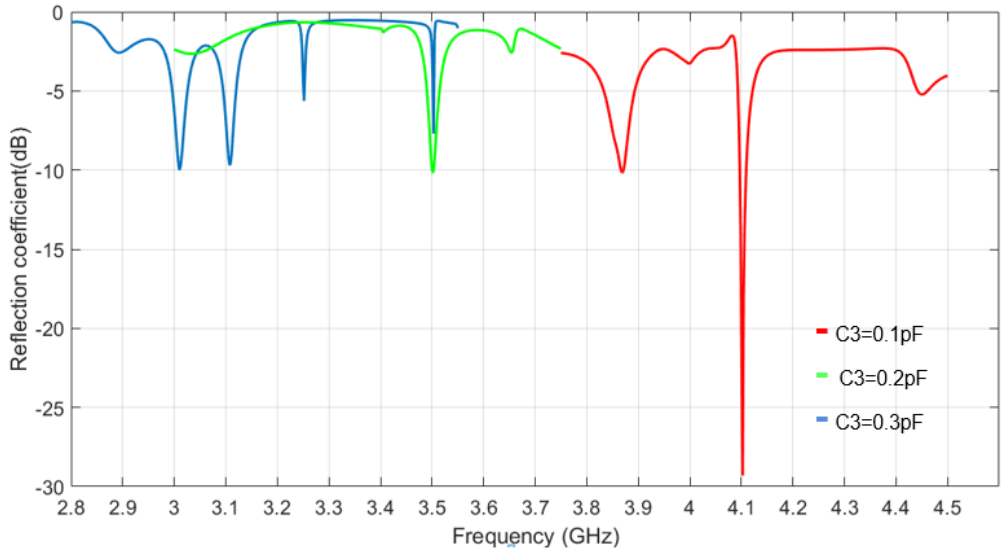


Figure 4.20: Reflection coefficient of frequency tunable antenna for $C3$ = 0.1pF, $C3$ = 0.2pF, and $C3$ =0.3pF

## 4.9 Conclusion

A novel microstrip-based SIW slot antenna is demonstrated with reconfigurability in the form of a radiation pattern achieved using the integration of FPMS unit cells. The reference antenna design is explained with the help of simulated results throughout the work. The final design is optimized for impedance matching and radiation to show proof-of-concept for beam steering applications. The optimized antenna has a total length of 190 mm and a width of 80 mm, showing a beam steering of ±42° with a maximum gain of 6.1 dBi and a gain variation of 2 dB. Additionally, using the reference antenna design, polarization reconfigurability, and gain modulation are also studied. Exploiting the characteristics of FPMS technology, frequency tunability has also been explored for the SIW-slot antenna structure. The level of reconfigurability provided by the proposed antenna structure shows that FPMS can be used for the realization of smart and intelligent components for modern wireless applications.

# Chapter 5

# Conclusion and Future work

## 5.1 Conclusion

The future of modern wireless applications heavily relies on the incorporation of RF components that are low-cost, compact, and, last but not the least, agile. In the form of radiation pattern reconfigurability, this thesis shows one such smart antenna design that can cater for the needs of one such application. This thesis proposes a unique antenna design that incorporates FPMS unit cells into a slotted substrate integrated waveguide (SIW-slot) antenna to provide beam steering as well as frequency tuning.

The final optimized antenna has a length of 190 mm and a width of 80 mm when designed on Duroid 5880 with a thickness of 4.75 mm. FPMS unit cells are integrated into the active elements (i.e. the slots) of the reference antenna. All the simulations are performed with the help of the Ansys HFSS full-wave simulator. The simulations show a beam steering of ±42º with a maximum gain of 6.1 dBi at 4 GHz. The maximum gain variation of the antenna is 2 dB. Throughout the steering of antenna radiation, the antenna impedance remains generally matched which is highly desired for such an antenna system. Furthermore, antenna capabilities in terms of polarization reconfigurability and gain modulation is also investigated and analyzed. The antenna is observed to be switching its polarization from $\boldsymbol{E}_{\varphi}$ (maximum at -4°) to $\boldsymbol{E}_{\theta}$ (±42°)which helps to establish secure communication.

As a next step, the same antenna design is further modified to study its efficacy in frequency tunability. The new design does provide a frequency tunability of almost 25 % while maintaining antenna's gain and radiation characteristics.

## 5.2 Future Work

Many different adaptations, tests, and experiments can be drawn from the work that has been detailed in this thesis. However, the first and the most natural future step is to practically realize the proposed antenna designs and characterize them for their impedance and radiation performance. This will allow to provide a complete proof-of-concept for the reconfigurable antenna system with added frequency tuning capabilities. In order to achieve this goal the author has short-listed a couple of vendors that can help in the fabrication of the prototype. These vendors are Syber Circuits and Candor Inc. located near Toronto, ON. However, in order to get a quotation from these vendors, the antenna layout needs to be finalized as per their fabrication process. Once this process has been completed, then the fabrication of the antenna designs can be pursued. Fortunately, for the characterization of the antenna, Georgian College has a facility available known as the Antenna Anechoic Chamber. For now, this facility is configured for Electromagnetic Compatibility (EMC) but it can be easily modified to measure an antenna in this chamber. Therefore, it is anticipated that the antenna design can be tested here. In case this option does not pan out as planned, there are other options available for the antenna measurements. These include Polytechnique Montreal (University of Montreal) and University of Waterloo, both of which have the required facilities for such measurements.

In terms of exploring the design further, it would be interesting to study the effect of slot rotation further while tuning the unit cell properties. It is shown pictorially in Fig. 5.1 (a). Generally, SIW slot antenna radiates well when the slot is placed in the line of direction of propagation of wave,

however, by carefully modifying the unit cell placement, it is believed that a new dimension can be studied that can control the antenna performance matrix. Other than this, other antenna designs can also be studied using the FPMS design concept. One such design is a Horn antenna shown in Fig. 5.1 (b). The concept proposes a substrate-based horn antenna whose dimensions can be modulated by using FPMS unit cells. One idea is shown in Fig. 5.1 (b), however, several other techniques can be used to further enhance antenna characteristics. Thus, this work can be considered as a new door for the design and implementation of a new class of using FPMS technology.

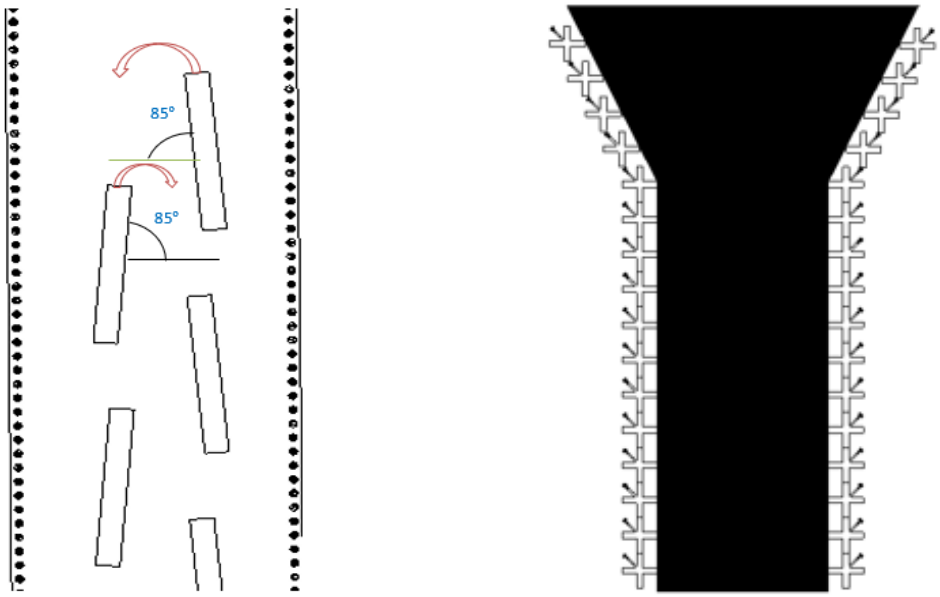


(a) (b)

Figure 5.1 Pictorial representation (a) Rotation of slots (b) FPMS unit cell integrated on the horn antenna

# Bibliography


[1] John Keller, “Radar technology looks to the future,” 2008. Accessed: May 24, 2022. [Online]. Available: https://www.militaryaerospace.com/communications/article/16706819/radar-technology-looks-to-the-future

[2] Ankara, “Contract Signed for KU-BANT Satellite Communication System-2 Project,” 2021. Accessed: May 24, 2022. [Online]. Available: https://www.raillynews.com/2021/04/ku-bant-uydu-muhabere-sistemi-2-projesi-icin-sozlesme-imzalandi/

[3] D. Barad, S. Behera, and L. singh, “Electronically Reconfigurable High-Gain Steerable Antenna for Mobile Satellite Communication,” *International Journal of Engineering Research*, vol. 5, pp. 827–830, May 2016

[4] Alex Lidow, “GaN Technology for the Connected Car,” *IEPC*, Sep. 26, 2016. https://epc-co.com/epc/GaNTalk/Post/13749/GaN-Technology-for-the-Connected-Car (accessed May 26, 2022).

[5] Y. Cassivi, L. Perregrini, P. Arcioni, M. Bressan, K. Wu, and G. Conciauro, “Dispersion characteristics of substrate integrated rectangular waveguide,” *IEEE Microwave and Wireless Components Letters*, vol. 12, no. 9, pp. 333–335, 2002

[6] S. R. Rengarajan, “Compound radiating slots in a broad wall of a rectangular waveguide,” *IEEE Transactions on Antennas and Propagation*, vol. 37, no. 9, pp. 1116–1123, 1989

[7] Paul Wade, *W1GHZ Microwave Antenna book* . 2001.

[8] Roland. A. Gilbert, “Waveguide Slot Antenna Arrays,” in *Antenna Engineering Hand book*, McGraw-Hil, 2007.

[9] L. Yan, W. Hong, G. Hua, J. Chen, K. Wu, and T. J. Cui, “Simulation and experiment on SIW slot array antennas,” *IEEE Microwave and Wireless Components Letters*, vol. 14, no. 9, pp. 446–448, 2004

[10] S. E. Hosseininejad and N. Komjani, “Optimum Design of Traveling-Wave SIW Slot Array Antennas,” *IEEE Transactions on Antennas and Propagation*, vol. 61, no. 4, pp. 1971–1975, 2013

[11] C. Zhao, X. Li, C. Sun, H. Huang, and Y. Liu, “Design of a Low-SLL SIW Slot Array Antenna With a Large Declination in Ka -Band,” *IEEE Access*, vol. 7, pp. 120541–120547, 2019

[12] A. Dewantari, J. Kim, I. Scherbatko, and M.-H. Ka, “A Sidelobe Level Reduction Method for mm-Wave Substrate Integrated Waveguide Slot Array Antenna,” *IEEE Antennas and Wireless Propagation Letters*, vol. 18, no. 8, pp. 1557–1561, 2019

[13] P. Chen, W. Hong, Z. Kuai, and J. Xu, “A Substrate Integrated Waveguide Circular Polarized Slot Radiator and Its Linear Array,” *IEEE Antennas and Wireless Propagation Letters*, vol. 8, pp. 120–123, 2009

[14] D. Kim, W. Chung, C. Park, S. Lee, and S. Nam, “Design of a 45^-Inclined SIW Resonant Series Slot Array Antenna for Ka -Band,” *IEEE Antennas and Wireless Propagation Letters*, vol. 10, pp. 318–321, 2011

[15] W. Cao, W. Hong, Z. N. Chen, B. Zhang, and A. Liu, “Gain Enhancement of Beam Scanning Substrate Integrated Waveguide Slot Array Antennas Using a Phase-Correcting Grating Cover,” *IEEE Transactions on Antennas and Propagation*, vol. 62, no. 9, pp. 4584–4591, 2014

[16] Y.-Q. Wen, B.-Z. Wang, and X. Ding, “Wide-Beam SIW-Slot Antenna for Wide-Angle Scanning Phased Array,” *IEEE Antennas and Wireless Propagation Letters*, vol. 15, pp. 1638–1641, 2016

[17] A. Nafe, F. A. Ghaffar, M. F. Farooqui, and A. Shamim, “A Ferrite LTCC-Based Monolithic SIW Phased Antenna Array,” *IEEE Transactions on Antennas and Propagation*, vol. 65, no. 1, pp. 196–205, 2017

[18] N. Jess, B. A. Syrett, and L. Roy, “The Field-Programmable Microwave Substrate,” *IEEE Transactions on Microwave Theory and Techniques*, vol. 64, no. 11, pp. 3469–3482, 2016

[19] H. C. Mohanta, A. Kouzani, and S. Mandal, “Reconfigurable Antennas and Their Applications,” *Universal Journal of Electrical and Electronic Engineering*, vol. 6, pp. 239–258, May 2019

[20] P. K. Li, Z. H. Shao, Q. Wang, and Y. J. Cheng, “Frequency- and Pattern-Reconfigurable Antenna for Multistandard Wireless Applications,” *IEEE Antennas and Wireless Propagation Letters*, vol. 14, pp. 333–336, 2015

[21] J. Costantine, Y. Tawk, S. E. Barbin, and C. G. Christodoulou, “Reconfigurable Antennas: Design and Applications,” *Proceedings of the IEEE*, vol. 103, no. 3, pp. 424–437, 2015

[22] T. Li, H. Zhai, X. Wang, L. Li, and C. Liang, “Frequency-Reconfigurable Bow-Tie Antenna for Bluetooth, WiMAX, and WLAN Applications,” *IEEE Antennas and Wireless Propagation Letters*, vol. 14, pp. 171–174, 2015

[23] C. Sun, H. Zheng, L. Zhang, and Y. Liu, “A Compact Frequency-Reconfigurable Patch Antenna for Beidou (COMPASS) Navigation System,” *IEEE Antennas and Wireless Propagation Letters*, vol. 13, pp. 967–970, 2014

[24] Abdurahman Hmouda, “Frequency Reconfigurable Antennas for Airborne Applications,” Université du Québec , Qubec, 2017.

[25] Y. Li, Q. Xue, E. K.-N. Yung, and Y. Long, “Fixed-Frequency Dual-Beam Scanning Microstrip Leaky Wave Antenna,” *IEEE Antennas and Wireless Propagation Letters*, vol. 6, pp. 444–446, 2007

[26] I. Serhsouh, M. Himdi, H. Lebbar, and H. Vettikalladi, “Reconfigurable SIW Antenna for Fixed Frequency Beam Scanning and 5G Applications,” *IEEE Access*, vol. 8, pp. 60084–60089, 2020

[27] Z.-Y. Wen, Y.-L. Ban, Y. Yang, and Q. Wen, “Risley-Prism-Based Dual-Circularly Polarized 2-D Beam Scanning Antenna With Flat Scanning Gain,” *IEEE Antennas and Wireless Propagation Letters*, vol. 20, no. 12, pp. 2412–2416, 2021

[28] M. Bozzi, F. Xu, D. Deslandes, and K. Wu, “Modeling and Design Considerations for Substrate Integrated Waveguide Circuits and Components,” in *2007 8th International Conference on Telecommunications in Modern Satellite, Cable and Broadcasting Services*, 2007, p. P-VII-P-XVI

[29] P. Loghmannia, M. Kamyab, M. Ranjbar Nikkhah, and R. Rezaiesarlak, “Miniaturized Low-Cost Phased-Array Antenna Using SIW Slot Elements,” *IEEE Antennas and Wireless Propagation Letters*, vol. 11, pp. 1434–1437, 2012

[30] M. A. Kossel, R. Kung, H. Benedickter, and W. Biichtokd, “An active tagging system using circular-polarization modulation,” *IEEE Transactions on Microwave Theory and Techniques*, vol. 47, no. 12, pp. 2242–2248, 1999

[31] D. Piazza, J. Kountouriotis, M. D’Amico, and K. R. Dandekar, “A technique for antenna configuration selection for reconfigurable circular patch arrays,” *IEEE Transactions on Wireless Communications*, vol. 8, no. 3, pp. 1456–1467, 2009

[32] J. Yang, W. Lin, and H. Wong, “Wideband CP Polarization and Pattern Reconfigurable Antennas,” in *2018 IEEE International Conference on Computational Electromagnetics (ICCEM)*, 2018, pp. 1–2.

[33] W. Lin and H. Wong, “Wideband Circular Polarization Reconfigurable Antenna,” *IEEE Transactions on Antennas and Propagation*, vol. 63, no. 12, pp. 5938–5944, 2015,

[34] N. K. Roy and F. Abdul Ghaffar, “A Novel Microstrip Line Based Leaky Wave Antenna using Capacitive Loading,” in *2021 IEEE 19th International Symposium on Antenna Technology and Applied Electromagnetics (ANTEM)*, 2021, pp. 1–2.

[35] E. Ali, “Design substrate integrated waveguide slot array antenna at x-band,” 2013.

[36] J. Kachhia, A. Patel, A. Vala, R. Patel, and K. Mahant, “Logarithmic Slots Antennas Using Substrate Integrated Waveguide,” *International Journal of Microwave Science and Technology*, vol. 2015, p. 629797, 2015

[37] T. Djerafi, A. Doghri, and K. Wu, “Substrate Integrated Waveguide Antennas,” 2015, pp. 1–60. doi: 10.1007/978-981-4560-75-7_57-1.

[38] D. Deslandes and K. Wu, “Accurate modeling, wave mechanisms, and design considerations of a substrate integrated waveguide,” *IEEE Transactions on Microwave Theory and Techniques*, vol. 54, no. 6, pp. 2516–2526, 2006

[39] Robert. S. Elliot, *Antenna Theory and Design*. Englewood Cliffs: Prentice-Hall, 1981.

[40] D. Deslandes and K. Wu, "Accurate modeling, wave mechanisms, and design considerations of a substrate integrated waveguide," *IEEE Transactions on Microwave Theory and Techniques*, vol. 54, no. 6, pp. 2516–2526, 2006

[41] W.H Watson., "Resonant slots," *Journal of the Institution of Electrical Engineers-Part IIIA: Radiolocation*, vol. 93, no. 4, pp. 747–777, 1946.

[42] D. Deslandes and K. Wu, "Integrated microstrip and rectangular waveguide in planar form," *IEEE Microwave and Wireless Components Letters*, vol. 11, no. 2, pp. 68–70, 2001

[43] A. F. Stevenson, "Theory of Slots in Rectangular Wave-Guides," *Journal of Applied Physics*, vol. 19, pp. 24–38, 1948.

[44] A. J. Farrall and P. R. Young, "Integrated waveguide slot antennas," *Electronics Letters*, vol. 40, pp. 974–975, 2004.

[45] F. Xu and K. Wu, "Guided-wave and leakage characteristics of substrate integrated waveguide," *IEEE Transactions on Microwave Theory and Techniques*, vol. 53, no. 1, pp. 66–73, 2005

[46] C. J. Panagamuwa, A. Chauraya, and J. C. Vardaxoglou, "Frequency and beam reconfigurable antenna using photoconducting switches," *IEEE Transactions on Antennas and Propagation*, vol. 54, no. 2, pp. 449–454, 2006

[47] E. Erdil, K. Topalli, M. Unlu, O. A. Civi, and T. Akin, "Frequency Tunable Microstrip Patch Antenna Using RF MEMS Technology," *IEEE Transactions on Antennas and Propagation*, vol. 55, no. 4, pp. 1193–1196, 2007

[48] S. Missaoui, S. Missaoui, and M. Kaddour, "Tunable microstrip patch antenna based on liquid crystals," in *2016 XXIst International Seminar/Workshop on Direct and Inverse Problems of Electromagnetic and Acoustic Wave Theory (DIPED)*, 2016, pp. 88–91.

[49] L. F. Chen, *Microwave electronics : measurement and materials characterization*. Chichester: Wiley, 2004.